In situ measurements of post-fire debris flows in southern California: Comparisons of the timing and magnitude of 24 debris-flow events with rainfall and soil moisture conditions

Jason W. Kean,[1] Dennis M. Staley,[1] and Susan H. Cannon[1]

Received 25 February 2011; revised 12 August 2011; accepted 17 August 2011; published 5 November 2011.

[1] Debris flows often occur in burned steeplands of southern California, sometimes causing property damage and loss of life. In an effort to better understand the hydrologic controls on post-fire debris-flow initiation, timing and magnitude, we measured the flow stage, rainfall, channel bed pore fluid pressure and hillslope soil-moisture accompanying 24 debris flows recorded in five different watersheds burned in the 2009 Station and Jesusita Fires (San Gabriel and Santa Ynez Mountains). The measurements show substantial differences in debris-flow dynamics between sites and between sequential events at the same site. Despite these differences, the timing and magnitude of all events were consistently associated with local peaks in short duration (< = 30 min) rainfall intensity. Overall, debris-flow stage was best cross-correlated with time series of 5-min rainfall intensity, and lagged the rainfall by an average of just 5 min. An index of debris-flow volume was also best correlated with short-duration rainfall intensity, but found to be poorly correlated with storm cumulative rainfall and hillslope soil water content. Post-event observations of erosion and slope stability modeling suggest that the debris flows initiated primarily by processes related to surface water runoff, rather than shallow landslides. By identifying the storm characteristics most closely associated with post-fire debris flows, these measurements provide valuable guidance for warning operations and important constraints for developing and testing models of post-fire debris flows.

Citation: Kean, J. W., D. M. Staley, and S. H. Cannon (2011), In situ measurements of post-fire debris flows in southern California: Comparisons of the timing and magnitude of 24 debris-flow events with rainfall and soil moisture conditions, *J. Geophys. Res.*, *116*, F04019, doi:10.1029/2011JF002005.

1. Introduction

[2] In southern California, the combination of mountainous terrain, dense population, and high fire-frequency put new areas at risk to debris flows almost every year. These events often damage property [e.g., *McPhee*, 1989; *Lin et al.*, 2010] and sometimes cause fatalities, such as on Christmas Day 2003, when debris flows from burned areas above San Bernardino killed 16 people [*Chong et al.*, 2004]. A particularly hazardous aspect of post-fire debris flows is that they can be triggered by much less rainfall than is required for debris-flow initiation in unburned areas [*Cannon et al.*, 2008].

[3] Rainfall intensity-duration thresholds are a standard method to forecast debris flows and landslides [e.g., *Guzzetti et al.*, 2008; *Baum and Godt*, 2010]. In southern California, empirical rainfall intensity-duration thresholds for post-fire debris flows [*Cannon et al.*, 2008, 2011] are used in a debris-flow warning system operated by the National Oceanic and Atmospheric Association (NOAA) and the U.S. Geological Survey (USGS) [*NOAA-USGS Debris Flow Task Force*, 2005]. While sufficient data have now been collected to define reliable post-fire rainfall-intensity thresholds for parts of southern California, such as the San Gabriel Mountains [*Cannon et al.*, 2011], the data are not adequate to identify the rainfall characteristics most closely associated with these events. Consequently, like most rainfall-intensity duration thresholds, the southern California thresholds are defined for a wide range of durations (5 min to 24 h) in order to accommodate various combinations of rainfall intensity and duration that might trigger debris flows: from short duration, high-intensity rain bursts to long duration, lower intensity rainfall. The range of combinations reflects the assumption that triggering conditions may depend on additional factors, such as basin topographic and burn characteristics, soil properties and water content, and debris-flow initiation processes. Understanding these effects requires a combination of site characterization, field observations, and direct measurements of the hydrologic conditions leading up to and during debris flows.

[4] Unfortunately, the steep terrain and sporadic nature of debris-flow occurrence have limited the collection of direct measurements of natural debris flows to only a few sites

[1]U.S. Geological Survey, Denver, Colorado, USA.

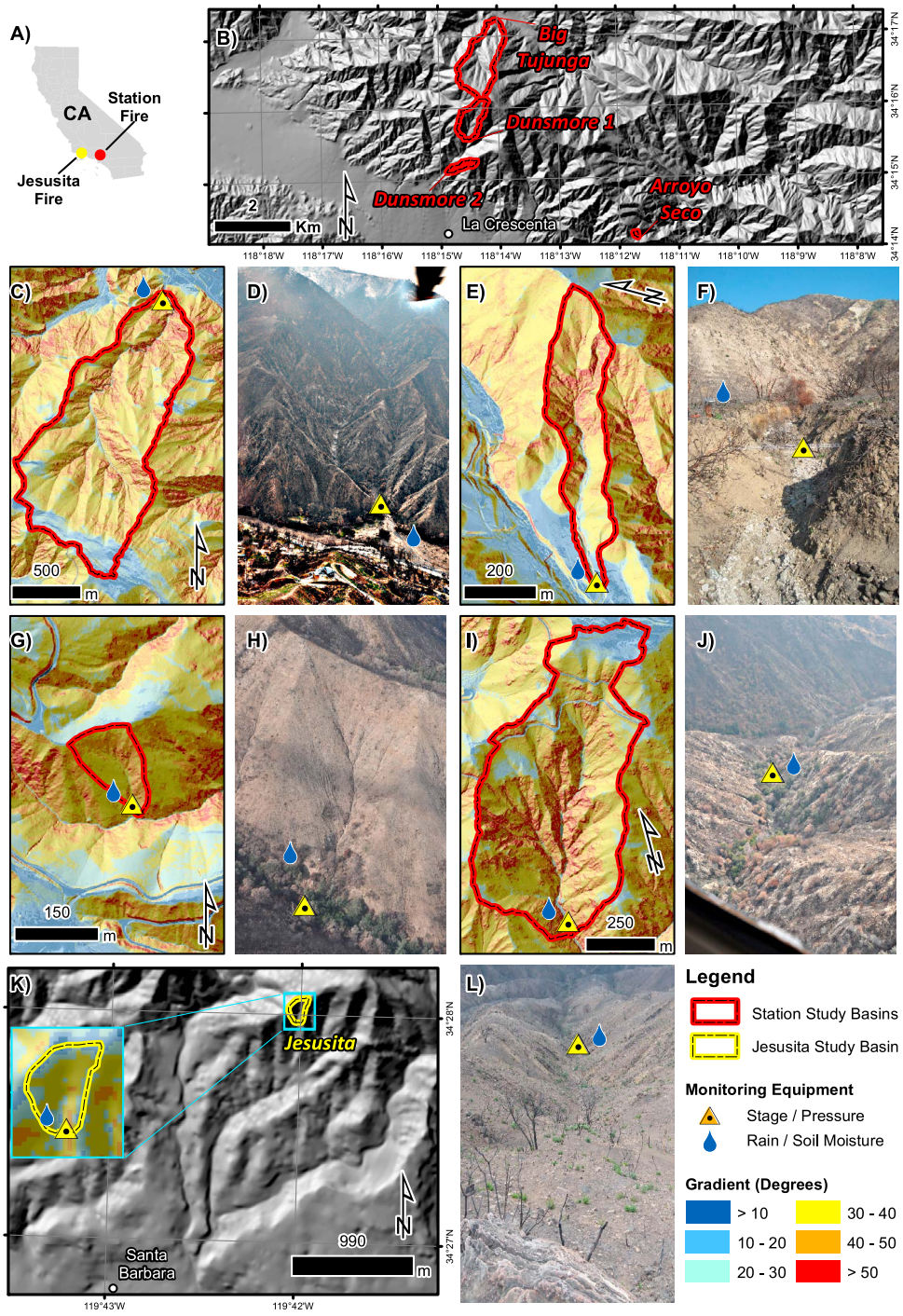

Figure 1. Study area. (a) Locations of the Station Fire (San Gabriel Mountains, red) and Jesusita Fire (Santa Ynez Mountains, yellow). (b) Site locations in the San Gabriel Mountains. Basin maps and photos of San Gabriel sites: (c–d) Big Tujunga, (e–f) Dunsmore 2, (g–h) Arroyo Seco, and (i–j) Dunsmore 1. (k–l) Site location, basin map, and photo of Jesusita site in the Santa Ynez Mountains. The triangle on the maps and photos is the location of the stage gage at the outlet of the drainage area. The raindrop is the location of the soil moisture sensors and/or rain gage. The basins maps for the San Gabriel sites are generated from a 2-m DEM; the map for the Santa Ynez site is from a 10-m DEM.

worldwide [*Zhang*, 1993; *Berti et al.*, 2000; *Marchi et al.*, 2002; *Hürlimann et al.*, 2003; *McArdell et al.*, 2007, *Berger et al.*, 2011, *Suwa et al.*, 2009; *McCoy et al.*, 2010]. These sites are all in unburned areas with consistent high rates of debris-flow activity. The transient aspects of fire present two additional difficulties to obtaining measurements in burned areas. First, the time window available to install measurement equipment after the fire and before the

Table 1. Summary of Site Characteristics

Site	Range	Latitude/ Longitude[a] (UTM)	Basin Area, A_b (km^2)	Basin Length From Outlet to Divide[b], L_b (m)	Area Burned At Moderate/High Severity [c] (%)	Max/Min Elevation[b] (m)	50th/90th Percentile Basin Slope[b] (deg)	Channel Slope at Station[d] (deg)
Arroyo Seco	San Gabriel	3788964/389956	0.0135	206	99	1040/940	39/46	22
Jesusita	Santa Ynez	3817186/251989	0.0224	250	100	540/429	30/36	14
Dunsmore 2	San Gabriel	3790898/385225	0.0795	734	66	1149/817	39/50	12
Dunsmore 1	San Gabriel	3791625/385649	0.475	1415	43	1548/989	38/51	19
Big Tujunga	San Gabriel	3794688/386462	1.37	3030	97	1548/571	38/48	9

[a]Zone 11, NAD83.
[b]From 2-m DEM at all sites except Jesusita, which is from a 10-m DEM.
[c]Station and Jesusita Fire Burned Area Emergency Response Teams (written communication).
[d]Over 10 m from a total station survey.

first storm is short (typically days to months); and second, the period for data collection in southern California is relatively brief, because regrowth of vegetation substantially reduces the likelihood of debris flows after two years [*Cannon et al.*, 2008]. Consequently, measured time series of post-fire runoff is scarce and mainly limited to floods, such as those measured at streamflow gaging stations on high-order tributaries [e.g., *Moody and Martin*, 2001a; *Malmon et al.*, 2007]. Although some information on post-fire debris-flow timing is available from eyewitness accounts [e.g., *Cannon et al.*, 2001; *Larsen et al.*, 2006], this information is often temporally imprecise and rarely accompanied by detailed hydrologic data.

[5] In the absence of direct measurements of post-fire debris flows, post-event field observations provide clues to the triggering conditions. These observations have shown that post-fire debris flows can be generated by a variety of processes including entrainment of hillslope and channel material initiated by surface water runoff [*Meyer and Wells*, 1997; *Cannon et al.*, 2001; *Gabet and Bookter*, 2008; *Santi et al.*, 2008; *Nyman et al.*, 2011], small centimeter-scale soil slips [*Wells*, 1987; *Gabet*, 2003], and meter-scale shallow landslides [*Rice and Foggin*, 1971; *Scott*, 1971; *Wondzell and King*, 2003]. *Meyer et al.* [2001] observed that in the Idaho batholith region there is a shift in the style of debris-flow initiation with time following the fire. They suggested in the first years after the fire, the debris flows were generated primarily from process related to surface water runoff from bare, burned hillslopes, whereas several or more years after the fire, following regrowth of herbaceous vegetation and loss of root strength, debris-flow initiation by shallow landslide failure was more likely. With some exceptions [e.g., *Scott*, 1971], field observations indicate the style of initiation of post-fire debris flows in southern California also shifts from runoff dominated [e.g., *Cannon et al.*, 2008; *Santi et al.*, 2008] to landslide dominated [e.g., *Rice and Foggin*, 1971] in the decade following the fire. Although the mechanics by which surface water flow transforms into debris flow are not well understood, direct measurements of runoff-initiated debris flows at multiple sites in unburned but sparsely vegetated basins show that the process occurs extremely rapidly in response to short-duration high-intensity rainfall [*Berti et al.*, 1999; *Suwa et al.*, 2009; *McCoy et al.*, 2010, 2011]. In contrast, meter-scale shallow landslides, which are triggered indirectly by rainfall through its effect on pore water conditions, can initiate from a much broader range of combinations of rainfall intensity and duration [*Caine*, 1980; *Guzzetti et al.*, 2008; *Baum and Godt*, 2010].

[6] We hypothesize that in the first year after the fire, when the probability of debris flow is highest [*Cannon et al.*, 2008], the timing of post-fire debris flows is consistently tied to the onset of high intensity rainfall capable of producing overland flow. To test this hypothesis we established debris-flow monitoring stations equipped with rain and non-contact stage gages to measure precisely the timing of flow relative to rainfall in five different southern California watersheds burned in 2009. In addition to testing this hypothesis, our monitoring strategy was designed to examine three more general questions concerning post-fire debris-flow hazards. (1) How does the debris-flow response change over the course of the first storm season following the fire? More specifically, what are the differences in timing, magnitude, and flow dynamics between debris flows in the first storm after the fire, when the channels are most loaded with sediment from dry ravel [*Wells*, 1987], and subsequent flows generated by storms later in the season? (2) How do storm rainfall accumulations and hillslope soil water contents affect debris-flow magnitude? More specifically, given similar triggering rainfall intensities, will debris flows that initiate at the beginning of a storm be different in magnitude than those that initiate later in a storm, because of differences in the water content of the hillslopes and channel bed sediments? And lastly, (3) how does the debris-flow response vary with basin scale and geologic material?

[7] During a series of storms in the first winter after the fires, our monitoring stations recorded measurements of rainfall, flow stage, hillslope soil water content, and channel bed pore fluid pressure accompanying 24 post-fire debris flows. This unique data set, in combination with post-event field observations and slope stability modeling, clearly identified the hydrologic triggering conditions of the debris flows and provided the information needed to test our hypothesis and begin to answer the above questions. In addition to providing guidance for warning operations, our measurements also provide valuable constraints for developing and testing future models of post-fire debris flow.

2. Study Sites

[8] We selected study sites that span two orders of magnitude in basin area and include two different mountain

Table 2. Timeline of Fires, Site Installation, and Debris-Flow Producing Storms

Date	Event	Affected Sites[a]
5–18 May 2009	Jesusita Fire	JS
25 August – 16 October 2009	Station Fire	AS, BT, D1, D2
30 September 2009	JS site installed	
9 October 2009	D1 site installed	
10 November 2009	AS site installed	
12 November 2009	Storm 1	AS (1)
24 November 2009	D2 site installed	
9 December 2009	BT site installed	
12–13 December 2009	Storm 2	AS (7), D1 (1), BT(1)
18 January 2010	Storm 3	AS(2), D1(1), D2 (1), BT (1)
18 January 2010	stage gage destroyed	BT, D1
1 February 2010	stage gage replaced	D1; *BT stage discontinued*
6 February 2010	Storm 4	AS(3), D1(2), D2(2)
27 February 2010	Storm 5	JS (1), D1(1)

[a]Number of recorded debris-flow events during storm. Arroyo Seco (AS), Jesusita (JS), Dunsmore 2 (D2), Dunsmore 1 (D1), Big Tujunga (BT).

ranges having different geologic materials (Figure 1 and Table 1). Four sites (Arroyo Seco, Dunsmore 1, Dunsmore 2, and Big Tujunga) were located along a 15-km portion of the San Gabriel Mountain Front adjacent to densely populated communities. This area was burned in the 650 km^2 Station fire of August and September 2009, the largest fire recorded in Los Angeles County history. A fifth site (Jesusita) was located in the Santa Ynez Mountains. This area was burned in the 35 km^2 Jesusita Fire of May 2009. We installed the monitoring instruments before significant rainfall in the months following the fires (see timeline in Table 2). At Arroyo Seco and Big Tujunga, the first debris flow occurred within a few days of installation. The short time window available for site selection and installation shown in Table 2 highlights one of the principal challenges of directly measuring post-fire debris flows.

[9] The sites share similar topographic characteristics (Table 1), climate (Mediterranean), and pre-fire vegetation (chaparral). The underlying bedrock of the San Gabriel sites is Cretaceous granitic rock [*Yerkes and Campbell*, 2005], whereas Eocene Coldwater Formation underlies the Santa Ynez site [*Minor et al.*, 2009]. Size distributions of the hillslope sediment at the five sites are shown in Figure 2a. The textural classification of the hillslope soils at the four San Gabriel sites is sand; the texture of hillslope soil at the Santa Ynez site is silty sand. In the months between the end of the fire and the first storm, there was substantial transport of hillslope sediment by dry ravel. This material contributed greatly to the supply of sediment in the channels.

[10] In the last hundred years, the San Gabriel Mountain Front has experienced several fires followed by storms that produced major debris flows [*Eaton*, 1935; *Scott*, 1971; *McPhee*, 1989]. The most damaging storm occurred on 31 December 1933 through 1 January 1934, prior to the development of Los Angeles County's network of debris basins along the mountain front. Debris flows during this storm killed at least 30 people and damaged or destroyed 483 homes in the communities of La Crescenta and Montrose [*Chawner*, 1934; *Eaton*, 1935]. Debris flows during the largest storm following the Station Fire (6 February 2010) overtopped several debris basins and damaged or destroyed 41 homes in the same area [*Lin et al.*, 2010]. The Santa Ynez Mountains also have a recent history of post-fire debris flows [*Wells et al.*, 1987; *Florsheim et al.*, 1991; *Gartner et al.*, 2008]. However, these debris flows have not caused as much damage as those in the San Gabriel Mountains, perhaps because the rainfall threshold for triggering debris flows in the Santa Ynez Mountains is higher

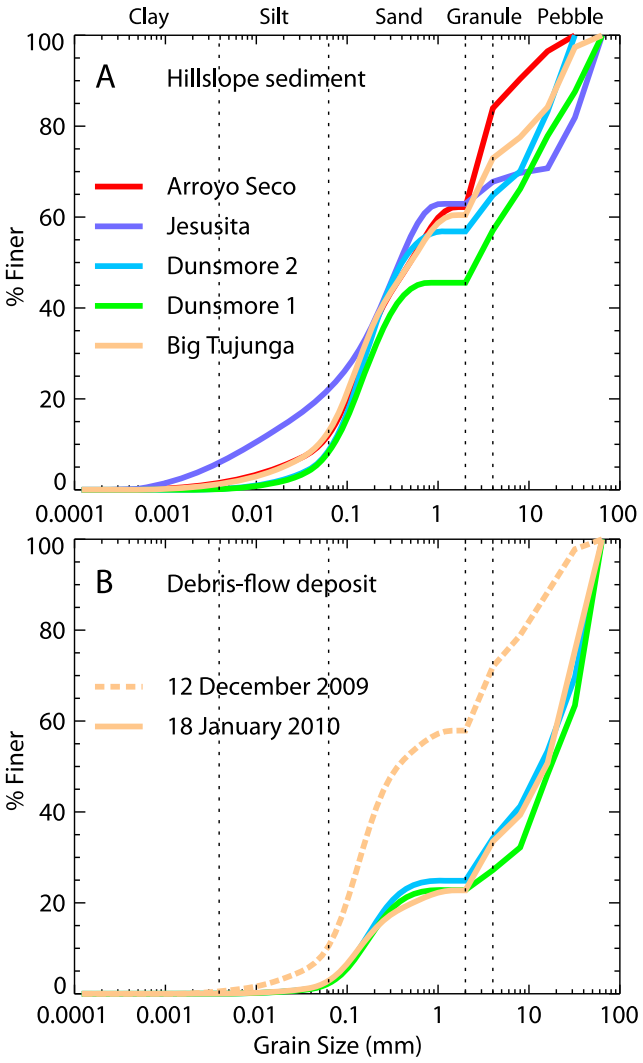

Figure 2. Size distributions of (a) hillslope sediment and (b) debris-flow deposits. Size fractions above 2 mm were determined by sieve analysis. Size fractions below 2 mm were analyzed by laser diffraction. The size distributions do not include clasts larger than 64 mm. The dashed line in Figure 2b is for the debris-flow deposit at Big Tujunga following the first event at the site on 12 December 2009. The solid lines in Figure 2b are for debris-flow deposits at Dunsmore 2, Dunsmore 1, and Big Tujunga following the debris flows on 18 January 2010. The 18 January 2010 debris flow was the first to occur at Dunsmore 2 and the second to occur at Dunsmore 1 and Big Tujunga.

Table 3. Sensor Specifications

Measurement	Make[a] and model	Sampling Rate	Accuracy/Resolution	Sites
Stage (laser)	SICK DT50-HI	10 Hz	±7 mm/1 mm	AS, BT, D1
Stage (sonic)	Campbell Scientific SR50A	2 s	±1 cm/1 mm	D2, JS
Pore pressure	Campbell Scientific CS450	2 s	±5 mm/1 mm (water depth)	All sites
Precipitation	Texas Electronics TR525	2 s	±1%/0.2 mm	All sites
Soil moisture	Decagon EC-5	1 min	±3%/0.001 m^3/m^3	All sites except BT
Video	Erdman Video Systems MiniBiscuit	4 frames/sec	640x480 pixels	D2

[a]Any use of trade or product names does not constitute endorsement by the U.S. Government.

than in the San Gabriel Mountains, as will be discussed in section 4.4.

3. Methods

3.1. Monitoring Stations

[11] Measurements at our monitoring stations include rainfall (R), flow stage (H), channel bed pore fluid pressure head (P), and hillslope soil water content (θ). The site Dunsmore 2 is also equipped with a rain-triggered video camera. Each station defined the outlet of the study basin. Our monitoring stations are similar to stations used at a long-term debris-flow monitoring site at Chalk Cliffs, Colorado [*McCoy et al.*, 2010, 2011]. Sensor specifications and sampling rates are given in Table 3, and a typical configuration of the sensors is shown in Figure 3. Photos of each of the monitoring stations are shown in Figure S1 of the auxiliary material.[1]

[12] We located the five stations on relatively straight, stable cross sections (Figure 4) to minimize error in estimates of flow cross-sectional area during an event (see section 3.2.3). We surveyed the cross sections and local channel slope at the time of installation with a total station. Repeat cross sections were surveyed after almost every debris-flow producing storm. These repeat cross sections documented the extent of channel change at the station and provided a new baseline cross section for computing flow cross-sectional area of subsequent events. Exposed bedrock made up the bottom of the cross section at Dunsmore 1 and the right side of the cross section at Big Tujunga. Partially exposed boulders (~1m in diameter) were present in the bottom of the Big Tujunga and Dunsmore 2, and a fully exposed boulder (~1m in diameter) made up part of the Jesusita cross section (Figure 4b). Colluvium and channel fill formed the remainder of the cross sections.

3.1.1. Stage and Channel Bed Pore Fluid Pressure

[13] To determine the timing and estimate the magnitude of the flows, we measured flow stage at each station (basin outlet) using laser (Arroyo Seco, Dunsmore 1, and Big Tujunga) and ultrasonic (Dunsmore 2 and Jesusita) distance meters. We suspended the distance meters above the channel by either portable bridges or horizontal poles anchored to one side of the channel. Two different types of sensors were used because of availability of equipment; however, the accuracy of both stage sensors is comparable (~1 cm). The main differences between the two sensors are that the laser can be sampled at a faster rate than the sonic sensor (10 Hz vs 2 s), and it has a smaller beam footprint (3 mm diameter vs 30 degree cone; equivalent to a 53 cm diameter at distance of 1 m). The higher frequency and smaller foot print of the laser make it better suited for measuring rapid stage changes in narrow channels than the sonic sensor; however the ultra-sonic meter has been shown by *McCoy et al.* [2010] to be adequate for measuring debris-flow stage in channels comparable in width to our two ultrasonic-equipped sites.

[14] We installed a vented pore pressure transducer in the channel bed at each site, and sampled them every 2 s during events. The elevation of the pressure transducer is the datum for the stage gage. At Dunsmore 1 and Big Tujunga the pressure transducer was anchored in exposed rock in the cross section. At the other three sites the pressure sensors were buried initially beneath 10 to 30 cm of loose bed material. The pressure transducer served several purposes. First, measurements of excess pore fluid pressure (pressure greater than hydrostatic) during a surge were used to help confirm the flow was a debris flow. Excess pore fluid pressures were usually only observed when the pressure transducer was located less than a few centimeters from the base of the flow. Second, when the pressure transducer was buried by bed sediment, it measured the level of the pre-

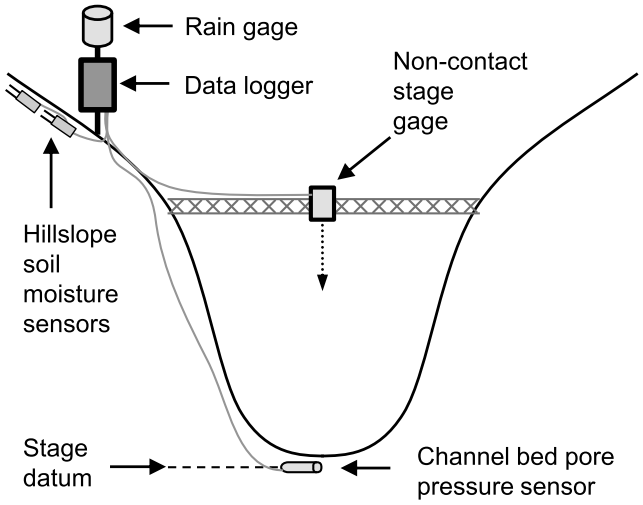

Figure 3. Diagram of debris-flow monitoring station. Non-contact stage gages are suspended over the channel. The datum for the stage gage is the level of a pore pressure sensor mounted in the channel bed. The data logger, rain gage, and soil moisture sensors are located on an adjacent hillslope above the stage gage and away from remaining vegetation (if any) in the channel bottom. Photographs of each of the five stations are shown in the auxiliary material.

[1]Auxiliary materials are available in the HTML. doi:10.1029/2011JF002005.

event groundwater table, and thus provided an indication of the degree of saturation of the bed. Last, the pore pressure transducer provided a redundant measure of flow timing, which we used to help interpret timing data from 7 other basins in the Station Fire that we were monitoring using small self-contained pressure transducers/data loggers [*Leeper et al.*, 2010].

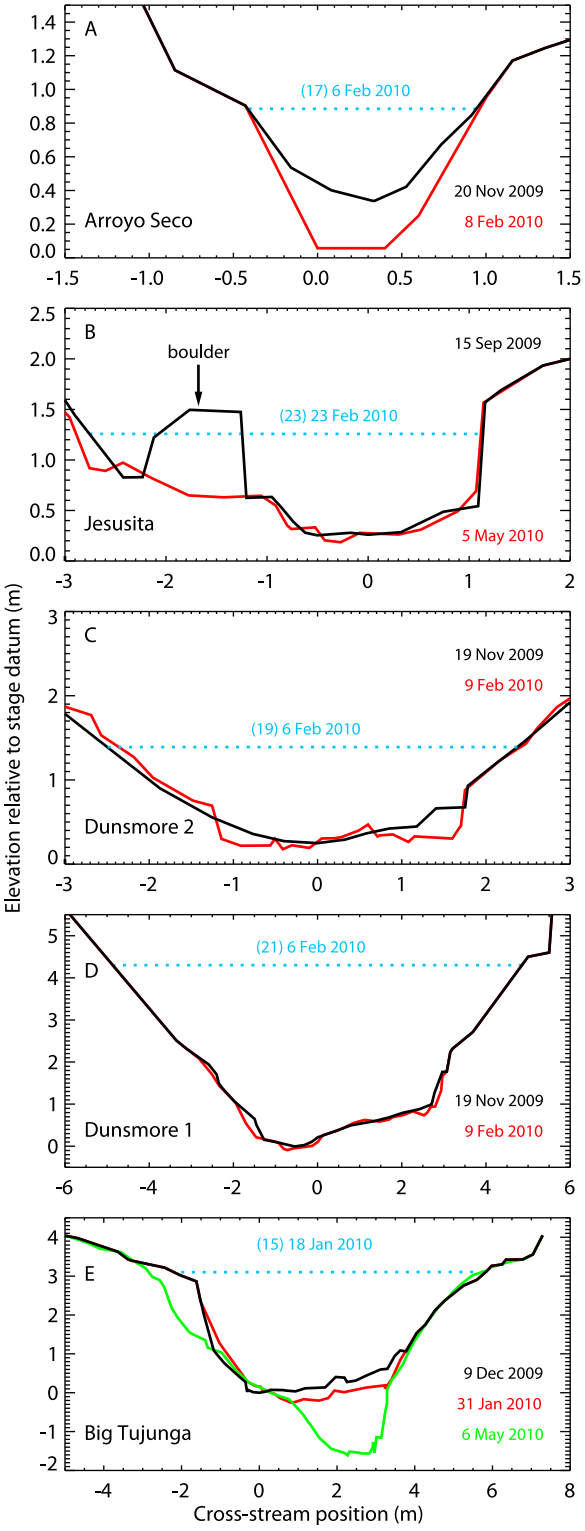

[15] The stage gages and pore pressure sensors at Dunsmore 1 and Big Tujunga were destroyed by debris flows on 18 January 2010. We installed a replacement laser stage gage at Dunsmore 1, but resources were not available to replace the Big Tujunga equipment. Only rainfall was measured at Big Tujunga after 18 January 2010. To avoid damage from future debris flows, we did not mount the Dunsmore 1 replacement laser directly over the channel. Instead, it was mounted on the side of the channel, 7-m above the bed, at a 36 degree angle from vertical. The oblique distance measurements were converted to stage by the cosine of the shot angle. As a result of the oblique shooting angle, which resulted in frequent missed laser returns, the effective sampling rate of stage was substantially less than 10 Hz. During good reflective conditions (typically high flow), the average sampling rate was approximately 0.5 Hz. At times of low or no flow, the laser often returned no data because of poor reflective conditions.

3.1.2. Rainfall

[16] We measured rainfall near the outlet of each study basin using a tipping-bucket rain gage that was sampled every 2 s. The rain gage was located at the station data logger, because it was used as a trigger for fast sampling of the stage and pore pressure sensors (stage and pore pressure were sampled at slow 1-min rates when it was not raining). Ideally, auxiliary rain gages would have been installed in the initiation areas of the study basins to account for spatial non-uniformity in rainfall. Unfortunately, installation of such gages did not occur at all sites because of time constraints. A second rain gage was installed near the ridge top of the Arroyo Seco basin. Data from this second rain gage are not used here, because it often (but not always) reported less rainfall than the rain gage at the station near the valley bottom. The difference in recorded rainfall between the ridge and station rain gages may have been due to systematically higher winds at the ridge, which would decrease the amount of rainfall intercepted by the rain gage. Given the very small basin areas (<0.08 km^2) of three of the study sites (Arroyo Seco, Jesusita, and Dunsmore 2), it unlikely that rainfall in the initiation areas of these basins deviated substantially from our measurements near the outlet.

Figure 4. Channel cross sections at monitoring stations. Sites were chosen to be at relatively stable cross sections in order to minimize uncertainties in estimates of flow cross-sectional area. Cross sections are drawn looking downstream and without any vertical exaggeration. The dashed blue line is the level of the highest stage measured at each station. The date and event number (Table 4) of this high flow is shown above the line. The black, red, and green dates correspond to the survey dates of the cross sections. The cross section at the time of site installation is shown with the black line. The cross section after the last recorded event at each station (or second to last event in the case of Dunsmore 1) is shown with the red line. The green line in Figure 4e is a cross section measured after the Big Tujunga station was discontinued on 18 January 2010. Most of the channel change between the red and green cross sections in Figure 4e was likely caused by unmeasured debris flows on 6 February 2010.

[17] More substantial spatially non-uniform rainfall was likely to have occurred within the two largest study basins (Dunsmore 1 and Big Tujunga) than at the three smallest basins. To assess rainfall variability in Dunsmore 1 and Big Tujunga we compared rainfall measured at the two stations to data from another rain gage (DUN3) that was established as part of a separate study [*Jorgensen et al.*, 2011]. The DUN3 gage was located at an elevation of 1326 m in the upper part of the Dunsmore 1 basin and was 700 m from the drainage divide to the upper part of Big Tujunga. *Jorgensen et al.* [2011] report rainfall data for DUN3 in 5-min intervals for three debris-flow producing storms on 12 December 2009, 18 January 2010, and 6 February 2010. The timing of rainfall at the DUN3 gage and the Dunsmore 1 and Big Tujunga gages was similar, but the rainfall totals differed. The ratios of storm cumulative rainfall at Dunsmore 1 to storm cumulative rainfall at DUN3 for the three storms was 0.95, 1.42, and 1.20 (mean = 1.19, i.e., more rainfall was generally recorded at Dunsmore 1 than DUN3). Less difference was observed in the ratios of storm cumulative rainfall between Big Tujunga and DUN3 for the three storms (0.91, 1.17, 0.91; mean = 1.00). Based on these comparisons, we conclude that the rainfall measured at our Dunsmore 1 and Big Tujunga stations are sufficiently representative of the rainfall in the upper part of the basins for the purposes of comparing trends in debris-flow timing and magnitude relative to rainfall.

3.1.3. Hillslope Soil Water Content

[18] To determine the relation between hillslope soil water content and debris-flow magnitude, we measured the soil water content of the hillslope near the rain gage using two sensors placed 5 cm below the surface. We sampled soil moisture continuously at 1-min intervals and took the average of the two sensors. No soil moisture measurements were made at Big Tujunga.

3.1.4. Video

[19] To obtain a visual record of flow conditions and to compute debris-flow front velocities, we installed a rain-triggered video camera at Dunsmore 2. The camera recorded images at a rate of 4 frames per second. We measured debris-flow front velocities by noting the front travel time between pixels with known spatial coordinates, which were determined from a total station survey. Although rain-triggered floodlights were installed to observe nighttime flows, the illumination was not sufficient to measure front velocities at night. Consequently, front velocities were only determined from several surges during a daytime debris-flow event on 18 January 2010.

3.1.5. Field Visits and Event Identification

[20] We made site visits following each storm to download data, check instruments, resurvey cross sections, and examine flow deposits and erosion features. In addition to ground observations, aerial observations of the erosion response of the Station Fire sites were made by helicopter following the most intense storm on 6 February 2010.

[21] Both debris flows and debris floods (hyperconcentrated flows) were recorded during the monitoring period. Some debris-flow events contained multiple surges in rapid succession (less than one minute apart) others consisted of only a single surge. Distinct flow events within a single storm were distinguished by periods of at least 20 min of negligible flow. Flow events were classified as debris flows if unsorted and unstratified, matrix-supported debris-flow deposits or mud veneers were observed in the vicinity of the station or if the stage record had the large-amplitude front characteristics of debris-flow surges [*Pierson*, 1986; *Iverson*, 1997; *Hungr*, 2000]. The latter criterion was necessary, because there were often multiple debris flows at a site during a single storm. Only the 24 events identified as being debris flows are used in this analysis. The 5 flow events not meeting the above criteria were likely debris floods. Video observations at Dunsmore 2 show that periods of flood flow were also present in the recessional flow of debris-flow events. Ideally, the type of flow at all sites would have been quantified precisely by measuring time series of flow density using force plates, such as that of *McArdell et al.* [2007]. However, installation of these sensors was not feasible because of the high cost, limited access, and short time window available to install equipment.

3.2. Data Processing

3.2.1. Stage Data

[22] To remove anomalous stage data points, we lightly filtered the laser and sonic distance measurements. The 10-Hz laser stage data were processed using a median filter with a window size of 5 data points (0.5 s). The filter replaces each data point with the median of neighboring points contained in the window. This filter preserved the complex structure of the time series, but removed anomalously high and low readings, such as those caused by missed laser returns and returns from large splashes. The ultrasonic stage data was filtered based on a measure of the quality of the returned sonic signal as described by *McCoy et al.* [2010].

3.2.2. Stage–Rainfall Intensity Correlation

[23] To determine the timing of the events relative to rainfall, continuous time series of rainfall intensities (I_D) for different durations (D = 2, 5, 10, 15, 30, 60, and 180 min) were calculated from the cumulative rainfall data using a backward difference equation ($I_D = [R(t) - R(t - D)\ ]\ /D$, where R is cumulative rainfall and t is time). The peak rainfall intensity for each event was identified as the local maximum in I_D within ± 30 min of the time of peak stage. The time difference between peak stage and the peak I_D is one simple measure of the timing of debris flows relative to rainfall. This measure, however, can be difficult to interpret because in some cases the peak rainfall intensity occurs after the time of peak flow. A second, more informative, measure of the timing of the debris flows relative to rainfall was determined from an analysis of the cross correlation between stage and I_D. The cross correlation coefficient (C_{xy}) between two time series x and y (here, stage and I_D) is given by

$$C_{xy}(l) = \begin{cases} \frac{\sum_{i=0}^{n-|l|-1} (x_{i+|l|} - \bar{x})(y_i - \bar{y})}{\sqrt{s_x}\sqrt{s_y}}, l < 0 \\ \frac{\sum_{i=0}^{n-l-1} (x_i - \bar{x})(y_{i+l} - \bar{y})}{\sqrt{s_x}\sqrt{s_y}}, l \geq 0 \end{cases} \quad (1)$$

where l is the lag, $s_x = \sum_{i=0}^{n-1} (x_i - \bar{x})^2$, $s_y = \sum_{i=0}^{n-1} (y_i - \bar{y})^2$, n is the number of data points in the series, and $\bar{x}$ and $\bar{y}$ are the means of the two time series. The lag was applied in 1-min increments both forward and backward in time. The maximum cross correlation coefficient ($(C_{xy})_{\max}$) and corresponding time lag at this maximum ($l = t_{lag}$) were noted for

each event and duration. This time lag corresponds to the time shift that produced the best match in shape between the time series of stage and I_D. A negative t_{lag} means most of the rainfall preceded the flow; a positive t_{lag} indicates most of the rainfall came after the flow.

3.2.3. Volume index

[24] To identify relations between debris-flow magnitude and both measured rainfall characteristics and hillslope soil water content, we calculated an index of the total volume (sediment and water) of each event from the station data. Unfortunately, debris-flow volumes could not be measured directly, because flow velocity was not measured at all stations, and because the stations were not all located immediately above fans or debris basins that would permit volume to be computed from topographic surveys. In addition, most of the recorded debris flows mixed with flows from adjacent basins shortly downstream from the stations. In the absence of direct volume measurements, the volume index described below provided an objective way to make comparisons between the relative magnitudes of the events. A discussion of how the volume index compares to actual debris-flow volumes is presented in section 4.5.

[25] The volume index (V) was computed from the product of a characteristic velocity of the flow and the summation of flow cross-sectional area during the event as given by the equation

$$V = u_b \sum_{t=t_0}^{t_1} A_{xs}(t)\Delta t \tag{2}$$

where, t_0 and t_1 are the start and end times of the event, Δt is the time between stage measurements, $A_{xs}(t)$ is flow cross-sectional at the station at time t, and u_b is a characteristic velocity of the flow. Our definition for the characteristic velocity is based on our hypothesis that, in the first year after the fire, most debris flows (or their watery precursors) initiate almost immediately after the start of intense rainfall. We define u_b at the basin scale as $u_b = L_b/t_b$, where L_b is the length scale for the basin (distance along the main channel from the station to the divide), and t_b is a measure of the time between the start of intense rainfall and an observed debris flow at the station. An objective measure of this time scale is given by $t_b = D\text{-}t_{lag}$ for the 5-min rainfall intensity, which is the rainfall intensity found to have the highest cross correlation with stage as will be shown in section 4.3. For a debris flow that initiates both at the start of intense rainfall and at the top of the basin, u_b is nearly equivalent to the mean travel velocity from the top of the basin to the outlet. The degree to which u_b is a surrogate for actual flow velocity at the station cross section (u_{xs}) is assessed in section 4.3 using measurements of debris-flow velocity made at Dunsmore 2 with spatially referenced video.

[26] Flow cross-sectional area (A_{xs}) in equation (2) was estimated by computing the area bounded by the measured flow surface, the surveyed cross section, and an estimate of the base of the flow during the event. Despite an effort to locate stations on relatively stable cross sections, some channel change usually took place between the time of the pre-storm survey and the end of the event. Prior to an event the bottom of the cross section was sometimes altered by accumulation of dry ravel or erosion/deposition from previous debris flows during the same storm. To account for these changes, we adjusted the bottom of the pre-storm surveyed cross section to match the pre-event bed level measured by the stage gage. During an event we estimated the base of the cross section in two ways depending on erosion characteristics. At the site that experienced the most substantial channel change (Jesusita, event 23), we computed A_{xs} using the pre-event cross section until the time of peak flow, at which time it was assumed that the 1-m diameter boulder on the left side of the channel was incorporated into the debris flow (Figure 4b). We used the post-event surveyed cross section to compute A_{xs} for the remainder of the flow. For all of the other events, which experienced less dramatic channel change than Jesusita, we estimated the bottom of the cross section during the flow by linearly interpolating the base of the channel with time from the pre- and post-event bed surface measured by the stage gage. Multiple linear segments were used in cases where the stage readings likely matched the bed surface during brief periods of negligible flow between surges. It is unlikely that the true base of the flow followed our simple linear interpolation. For example, recent field measurements of debris-flow erosion rates show that erosion is punctuated by the passage of debris-flow fronts [*Berger et al.*, 2010, 2011]. While many of the debris-flow surges recorded in our study likely caused erosion, others resulted in deposition at the cross section. Given the complexity of the flow history, and the absence of timing information on erosion/deposition, simple linear interpolation of the flow base level is the best objective approximation available. The error in integrated flow cross-sectional area is probably greatest for the first event at the smallest site, which experienced the greatest percentage change in base level relative to peak stage. If all of the erosion for this event occurred with the first surge, rather than by the linearly interpolated base level, the volume index would be 1.8 times greater than the volume index based on a linear erosion rate with time.

[27] Two things should be noted about equation (2). First, the volume index does not account for variability in flow velocity during a debris flow, such as has been measured by *Suwa et al.* [1993] and *Arattano and Marchi* [2000]. And second, the velocity scale u_b would not yield a meaningful volume index for debris flows that initiate considerably after the start of intense rainfall. This situation could occur for a debris flow mobilized from a shallow landside that failed well after the peak rainfall upon adequate wetting of the failure surface from infiltration. A velocity scale more appropriate the latter situation would be $\sqrt{gR_{xs}}$, where R_{xs} is the hydraulic radius at the station cross section. This velocity scaling was used by *Iverson et al.* [1998] to estimate lahar inundation area.

[28] As mentioned above, the peak surges of 18 January 2010 destroyed the stage equipment at Dunsmore 1 and Big Tujunga. We estimated the unmeasured post-peak volume for these two events from a polynomial fit of the peak depth (peak flow thickness, h_p) and the summation of flow cross-sectional after the peak $\left(\left(\overline{A_{xs}}\right)_{post}\right)$ from 5 events with complete stage records at the two sites ($\left(\overline{A_{xs}}\right)_{post} = 88h_p^2 + 1200h_p$; $r^2 = 0.83$). This estimate was added to the calculated pre-peak summation of flow cross-sectional area and multiplied by u_b to obtain a total volume index.

Figure 5. Paired photographs of post-event erosion at (a and b) Arroyo Seco and (c and d) Dunsmore 1. The hillslope and channel erosion characteristics shown in the photographs are representative of the erosion we observed at the other study sites. Photos were taken on the dates listed in the figure, which were less than one week after a debris-flow. Common reference points in the two pairs of photos are shown with the white arrows. In Figure 5a hillslope rilling was very pronounced after the first storm and debris flow at Arroyo Seco. Post-event dry ravel can be seen beginning to refill the steep channel. In Figure 5b the second storm at Arroyo Seco substantially eroded the well-developed rill network shown in Figure 5a. Figures 5c and 5d show channel erosion 290 m downstream of the Dunsmore 1 station (upstream area = 1.45 km^2) caused by the 18 January 2010 and 6 February 2010 debris flows. The white brackets in Figures 5c and 5d show the height of a person standing in the photos.

3.3. Slope Stability

[29] To provide some insight into the rainfall conditions and slope characteristics required to initiate shallow landslides, we conducted a one-dimensional, infinite slope stability analysis of a section of hillslope at the site that received the highest and most intense rainfall (Arroyo Seco). This analysis complements our post-event field observations of erosion characteristics. We determined slope stability by calculating the ratio of basal Coulomb friction to gravitationally induced downslope basal driving stress. This ratio, or factor of safety (F_s), is given by the equation

$$F_s = \frac{\tan\phi}{\tan\alpha} + \frac{c - \psi(Z,t)\gamma_w \tan\phi}{\gamma_s Z \sin\alpha \cos\alpha} \quad (3)$$

where Z is the vertical coordinate direction, t is time, α is the slope angle, c is the soil cohesion, ϕ is the soil friction angle, γ_s is the soil unit weight, γ_w is the unit weight of groundwater, and ψ (Z,t) is the groundwater pressure head, which is a function of depth and time. Slope failure occurs when F_s is less than one. We used the model TRIGRS [*Baum et al.*, 2008, 2010] to calculate ψ (Z,t) in response to a measured time series of rainfall from the most severe storm of the monitoring period. TRIGRS extends the transient rainfall infiltration model by *Iverson* [2000] to accommodate unsaturated conditions and an impermeable basal boundary at depth $Z = d_Z$. We measured the parameters c, ϕ, and saturated hydraulic conductivity, K_s, needed for these calculations by conducting drained direct shear and hydraulic permeability laboratory tests of undisturbed samples of hillslope material.

4. Results

[30] In the first year after the fires, five storms with recurrence intervals of two years or less produced debris flows at the study sites (see timeline in Table 3). The first storm was an isolated convective storm that affected only the Arroyo Seco site. The subsequent storms were long duration frontal storms that affected multiple sites. No debris flows were observed in the second year after the fire. To provide context for describing the results from our monitoring stations, we first present an overview of field observations of runoff and post-event erosion. We then present examples of the monitoring data followed by analyses of debris-flow timing, magnitude, and slope stability.

4.1. Field Observations of Runoff and Erosion

[31] Field observations of runoff during storms and erosion characteristics after storms indicate the debris flows

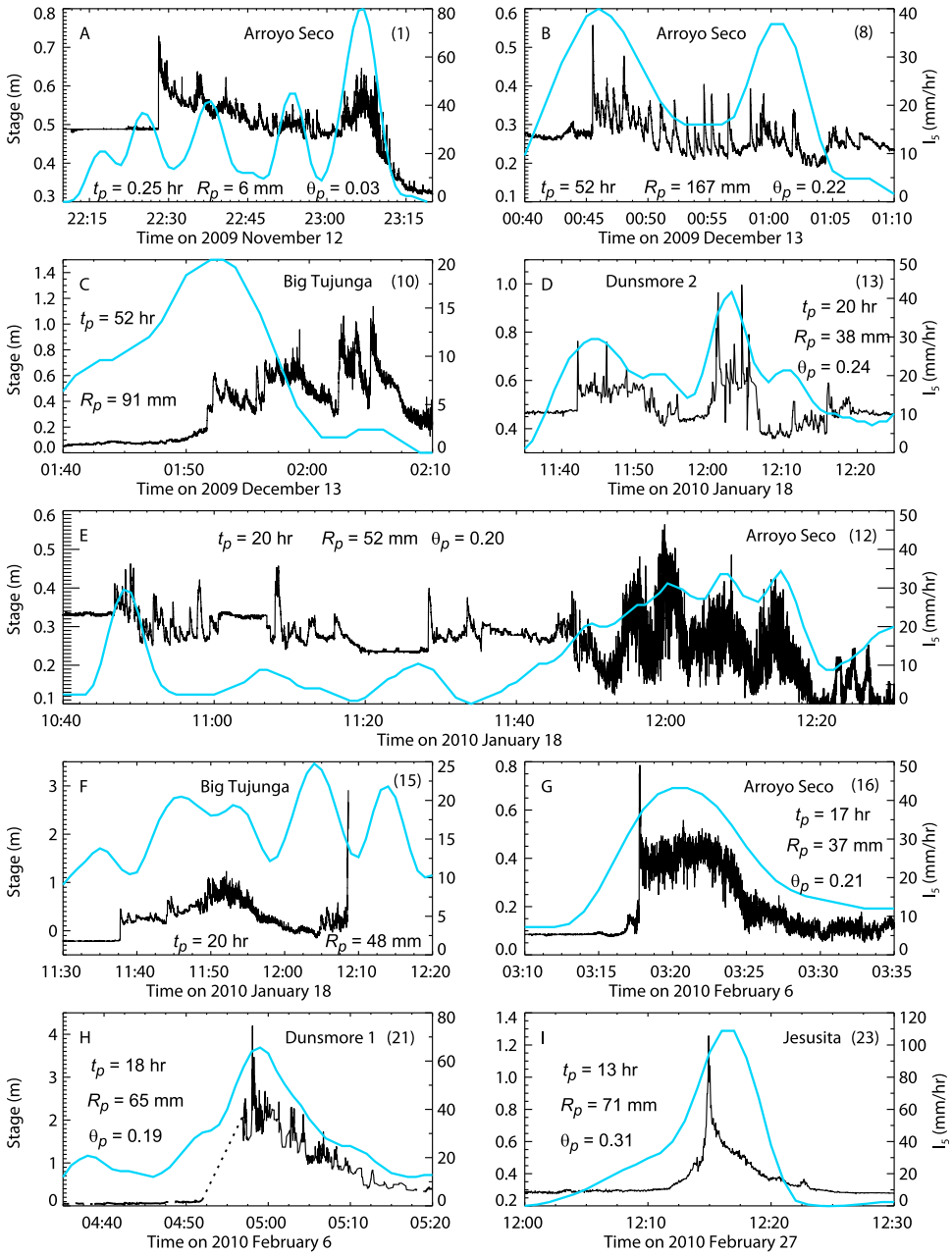

Figure 6. Representative examples of debris-flow events. Time series of stage (black line) and 5-min rainfall intensity (thick blue line). Time is in Pacific Standard Time. The values t_p, R_p and θ_p correspond to the storm duration, storm cumulative rainfall, and hillslope water content at the time of the peak flow. The number in parentheses corresponds to the event number listed in Table 4. The stage time series in Figure 6f ends at 12:08, because the stage sensor was destroyed by the flow. The dotted line in Figure 6h indicates a period of no stage data. Debris-flow events often contain multiple surges, and the timing of all events closely matches the timing of local peaks in rainfall intensity.

were initiated primarily by processes related to surface water runoff rather than by shallow landsliding. During storms, both eyewitness and video camera observations in the Station Fire documented widespread overland flow within minutes of intense rain bursts (I_5 = 20–26 mm/hr). Post-event aerial and ground-based visual observations of erosion documented that channel erosion and hillslope rilling were the dominant erosion features at all of the sites. Examples of these features are shown in Figure 5. These erosion characteristics are similar to erosion features documented by others in the first year after the fire [*Wells*, 1987; *Meyer and Wells*, 1997; *Shakesby and Doerr*, 2006; *Cannon et al.*, 2001; *Santi et al.*, 2008]. With the exception of some channel bank failures, very few meter-scale shallow landslide scars were observed, and these were outside of the study basins. However, sub-meter-scale soil failures of the

Table 4. Summary of Rainfall and Flow Characteristics for 24 Recorded Debris-Flow Events

Event Number	Date	Storm	Site	H_p (m)	I_{15p} (mm/hr)	t_p (hr)	R_p (mm)	θ_p (m^3/m^3)	θ_r (m^3/m^3)	Time of H_p (hh:mm:ss)	t_{lag} for I_{15} (min)	Time of I_{15p} (hh:mm)	Time of I_{15p} − Time of H_p (min)	Flow Duration (min)	u_b (m/s)	V (m^3)
1	12 Nov 2009	1	AS	0.73	30.4	0.25	6	0.03	0.03	22:28:08	6	22:37	9	50	0.6	240
2	12 Dec 2009	2	AS	0.59	25.6	42.8	91	0.22	0.13	14:47:57	−5	14:51	3	30	0.3	30
3	12 Dec 2009	2	AS	0.51	20.8	43.8	104	0.22	0.13	15:50:28	−1	15:59	9	20	0.5	30
4	12 Dec 2009	2	AS	0.47	19.2	44.7	114	0.22	0.13	16:42:03	−14	16:35	−7	60	0.2	10
5	12 Dec 2009	2	AS	0.43	16.0	46.3	131	0.22	0.13	18:19:13	−11	18:04	−15	15	0.2	4
6	12 Dec 2009	2	AS	0.50	19.2	47.2	139	0.22	0.13	19:10:43	−1	19:08	−3	25	0.5	20
7	12 Dec 2009	2	AS	0.50	24.0	51.8	155	0.21	0.13	23:50:02	1	23:37	−13	25	0.4	10
8	13 Dec 2009	2	AS	0.56	27.2	52.8	167	0.22	0.13	00:45:31	0	0:52	6	25	0.7	70
9	13 Dec 2009	2	D1	1.0	12.8	53.0	99	0.15	0.02	01:57:23	−5	1:55	−2	15	2.4	630
10	13 Dec 2009	2	BT	1.1	18.2	52.1	91	-	-	02:05:11	−5	1:55	−10	25	3.4	5600
11	18 Jan 2010	3	AS	0.56	12.0	17.8	37	0.21	0.09	09:48:29	−5	9:23	−25	45	0.2	120
12	18 Jan 2010	3	AS	0.56	30.4	20.0	52	0.2	0.09	11:59:37	6	12:13	13	110	0.9	210
13	18 Jan 2010	3	D2	1.0	27.4	20.0	38	0.24	0.07	12:04:22	6	12:10	6	40	2.0	710
14	18 Jan 2010	3	D1	2.8	35.2	20.0	52	0.2	0.08	12:03:39	0	11:50	−14	40	2.6	16000
15	18 Jan 2010	3	BT	3.1	20.6	20.1	48	-	-	12:08:34	0	12:13	4	40	4.6	36000
16	6 Feb 2010	4	AS	0.79	31.2	17.3	37	0.21	0.11	03:17:47	4	3:28	10	20	0.6	190
17	6 Feb 2010	4	AS	0.89	68.8	19.3	69	0.26	0.11	05:19:16	5	5:25	6	30	0.9	460
18	6 Feb 2010	4	AS	0.61	40.8	24.4	97	0.28	0.11	07:23:57	5	7:34	10	20	0.7	130
19	6 Feb 2010	4	D2	1.4	24.4	17.5	34	0.23	0.09	03:27:10	6	3:33	6	10	2.0	210
20	6 Feb 2010	4	D2	1.1	46.7	19.0	56	0.24	0.09	04:58:06	4	5:01	3	25	3.1	1000
21	6 Feb 2010	4	D1	4.3	47.2	19.0	65	0.19	0.13	04:58:04	3	5:03	5	30	3.9	35000
22	6 Feb 2010	4	D1	0.93	21.6	21.4	92	0.19	0.13	07:22:56	−4	7:19	−4	20	2.0	2200
23	27 Feb 2010	5	JS	1.3	56.0	13.3	71	0.29	0.14	12:14:56	1	12:17	2	20	1.0	380
24	27 Feb 2010	5	D1	1.8	32.8	6.2	43	0.05	0.05	07:14:24	−2	7:15	1	40	2.4	14000

type described by *Wells* [1987] and *Gabet* [2003] were observed by *Schmidt et al.* [2011] at the Arroyo Seco site following the first storm.

[32] In general, the station cross sections (Figure 4) experienced less channel change than parts of the channel elsewhere in the study basins. The lesser extent of change was due to our preference for locating cross sections at relatively stable sections in order to minimize errors in estimates of flow cross-sectional area. Figure 4 shows the cross section at the time of installation (black line), the cross section after the last recorded debris flow at the site (or second to last event in the case of Dunsmore 1) (red line), and the level of the highest stage recorded at the site during the monitoring period (blue dashed line). The green line in Figure 4e is for a cross section surveyed after the Big Tujunga station was discontinued. Most of the channel change between the red and green cross sections in Figure 4e is associated with unmeasured debris flows on 6 February 2010. Dunsmore 1 was the only site with exposed bedrock at the bottom of the cross section at the time of installation. Note the lack of cross-sectional change in the bedrock cross section of Dunsmore 1 is in stark contrast to the channel erosion shown in the photos in Figures 5c and 5d, which were taken 290 m downstream of the Dunsmore 1 station.

4.2. Monitoring Data and Event Variability

[33] Representative examples of debris-flow events from each of the five sites and each of the five storms are shown in Figure 6. The events are numbered with respect to the complete set of 24 recorded debris-flow events, which are summarized in Table 4 and shown in Figure S2 of the auxiliary material. Each plot shows time series of stage (H) and 5-min rainfall intensity (I_5). Figure 6 also lists, at the time of peak stage, the storm cumulative rainfall (R_p), hillslope soil water content (θ_p), and elapsed time since the start of the storm (t_p). Rainfall intensity is plotted for the 5-min duration, because it is the intensity measure that has the highest cross correlation with stage. Peaks in short-duration rainfall intensity associated with all events at the San Gabriel sites were at or above the previously published regional threshold of *Cannon et al.* [2008].

[34] In general, there is considerable variability and complexity to the measured stage time series. Estimates of peak flow depth range from 10 cm at Arroyo Seco (event 5, Figure S2 of the auxiliary material) to 4.3 m at Dunsmore 1 (event 21, Figure 6h). Events at many of the sites consist of multiple surges that occur at a higher frequency than fluctuations in 5-min rainfall intensity (e.g., event 8, Figure 6b). Other events, in contrast, consist of a single surge, such as the only debris-flow event recorded at Jesusita (event 23, Figure 6i). This event has stage characteristics similar to a flood hydrograph; however we confirmed the flow was a debris flow based on field evidence of matrix supported debris-flow deposits near the station. It should also be noted that the shape of the Jesusita stage time series may be affected by the removal of a 1-m diameter boulder from the cross section during the event (Figure 4b).

[35] In several cases the stage characteristics change substantially over the course of the event. Event 12 (Figure 6e) at Arroyo Seco is a good example of this aspect of the flow record. The first half of the event contains a series of small, short duration surges that are similar in appearance to those in (Figure 6b). At about 11:50 the flow changes dramatically with the appearance of relatively high frequency (~0.5 Hz), small amplitude stage fluctuations about a more gradually varying flow. The shift to a more agitated flow surface, which coincides with an increase in the rainfall intensity,

indicates there was an increase in the volume fraction of water in the flow. Since our sites were not equipped with force plates to measure flow density and quantify the water/sediment concentrations during these times, we do not know if the flow during such periods of high frequency stage fluctuations was a debris flow or debris flood. Similar combinations of distinct surges and periods of high frequency, small amplitude stage fluctuations are present in other events shown in Figure 6 (events 1, 15, and 16).

[36] At some sites, the stage characteristics also change over the course of the winter storm season. The seasonal change is most pronounced at the smallest site (Arroyo Seco) and is discussed in detail by *Kean and Staley* [2011]. The seasonal change coincides with the abrupt change in stage characteristics that occurs at about 11:50 during event 12 (Figure 6e), as described above. Prior events at Arroyo Seco have stage characteristics similar to those in the first half of event 12 (e.g., event 8, Figure 6b), whereas events after event 12 at Arroyo Seco are characterized by a single surge followed by periods of flow with high frequency stage fluctuations similar to those recorded in the second half of event 12 (e.g., event 16, Figure 6g). The change in stage characteristics is presumably related to the evolution of the drainage network and sediment supply during the winter storm season. The beginning of this evolution can be seen in the paired Arroyo Seco photographs in Figure 5. The first photo (Figure 5a) was taken after the first storm and debris flow at the site (event 1, Figure 6a). This storm created an extensive network of rills on the hillslopes. The second photograph (Figure 5b) was taken after the second storm, which produced a series of 7 events at Arroyo Seco ending with event 8 (Figure 6b). Close inspection of the second photograph shows that runoff during the second storm eroded much of the hillslope material that defined the rill boundaries formed during the first storm. The third storm at the site produced the transitional event 12 (Figure 6e). During a site visit after the third storm we observed that, while an ample supply of loose sediment remained on the hillslopes, there was a substantial increase in the amount of saprolite exposed on the hillslopes and bedrock exposed in the channels. Based on these observations, we suspect this exposure lead to an increase in the water content of the flow, which changed the stage characteristics from the surge dominated patterns recorded in the first half of the season to the rapid stage fluctuations often observed in the second half of the season.

[37] The largest site (Big Tujunga) also exhibited a distinct change in the stage characteristics between the first and second events at the site (events 10 and 15, Figures 6c and 6f). Both events had comparable rainfall intensity, and the first 30 min of the 18 January 2010 event is remarkably similar to the 13 December 2009 flow. The key difference between the two events is peak flow stage (H_p). The 18 January 2010 record ended with a 3.1-m high surge front that destroyed the stage and pressure gages, whereas the peak flow stage during the previous event was only 1.1 m. The large difference in H_p between these two events may be explained by the differences in both the grain-size distributions of the flow deposits and erosion characteristics near the station. Although both events transported boulders as large as 1 m, the debris-flow deposits of the first event were much finer grained than the deposits from the second event, as shown by the grain size distributions in Figure 2b. The sandy textured debris-flow deposits of the first event were deposited as a veneer along the channel margins near the station. The grain-size distribution of these deposits was very similar to the hillslope sediment (Figure 2a). This similarity indicates that the material likely came from hillslope rilling and erosion of channels loaded with dry ravel. The deposits from the second event, in contrast, were dominated by pebbles and cobbles (the cobble and larger size fractions are not represented in the grain-size analysis in Figure 2b). We also observed much greater channel bed and bank erosion in the vicinity of the station after the 18 January 2010 event than after the 13 December 2009 debris flow. Channel erosion after the 18 January 2010 event was similar in character to the erosion shown in Figure 5c at Dunsmore 1. Based on these observations, we conclude the shift to larger grain size of the deposits between the first and second events at Big Tujunga was caused by the addition of large clasts from erosion of the channel bed and banks.

[38] The formation of the 3.1-m deep surge front toward the end of the 18 January 2010 event was likely caused by the addition of these larger clasts to the flow. Grain-size segregation processes tend to sort larger clasts to the front of debris flows [e.g., *Pierson*, 1986]. The higher hydraulic diffusivity of the coarse particles results in lower fluid pressures at the front of the debris flow relative to tail [*Iverson*, 1997]. The longitudinal distribution of grain size and fluid pressures creates a gradient in flow resistance that decreases from the front to the tail. This gradient in flow resistance promotes the formation of steep surge fronts [*Hungr*, 2000], such as the one shown in Figure 6f. It is possible that the 13 December 2009 event did not produce such a high surge front, because it lacked enough large clasts to create a substantial gradient in flow resistance.

[39] The substantial shift to larger grain size deposits between the first and second event at Big Tujunga was observed in other unmonitored basins nearby, but not at all of the study sites. For example, the first event recorded at Dunsmore 2 on 18 January 2010 had a measured grain-size distribution similar to the second events at Big Tujunga and Dunsmore 1, as shown in Figure 2b. At Dunsmore 1, the unsampled flow deposit from the first event on 12 December 2009, which occurred within minutes of the first Big Tujunga event, was visually intermediate in texture to measured deposits of the first Big Tujunga event and the second 18 January 2010 event at Dunsmore 1. The control of grain size on flow dynamics and the observed variability in deposit grain size between sites and storms highlights a major challenge for predicting the peak depth of post-fire debris flows.

[40] Another aspect of variability in the data set is that the events took place over a wide range of times into the storm ($0.25 < t_p < 52$ h) and over a range of hillslope soil water contents ($0.03 < \theta_p < 0.31$). For example at Arroyo Seco, one event (Figure 6a) occurred just 15 min into a short thunderstorm after only 6mm of rainfall was recorded at both the station gage and the auxiliary rain gage at the top of the basin. At this time, the measured hillslope soil water content was nearly dry ($\theta_p = 0.03$) and equal to the pre-storm residual soil water content, θ_r. The hydrologic and erosion response of the upper part of the basin during this event is described in detail by *Schmidt et al.* [2011]. In contrast, at same site during the next storm, which lasted more than 2

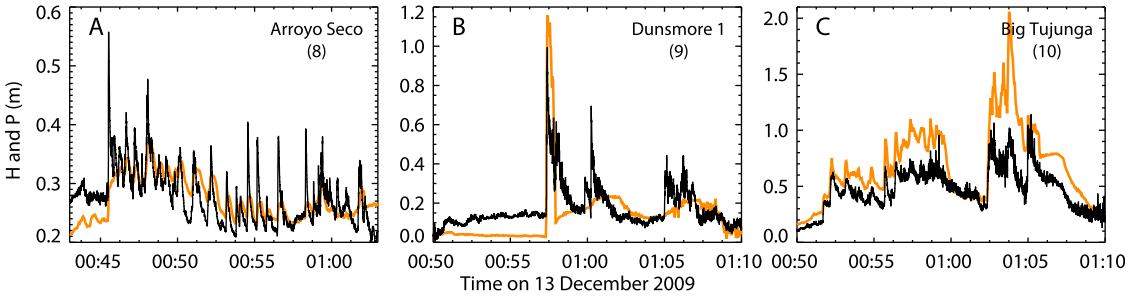

Figure 7. Example measurements of pore pressure head (P, thick orange line) and stage (H, black line) at (a) Arroyo Seco, (b) Dunsmore 1, and (c) Big Tujunga during storm 2. Excess pore pressures were measured in Figures 7b and 7c by sensors that were in direct contact with the flow. The pressure signal in Figure 7a is muted, because it was buried beneath 20 cm of partially saturated sediment. The number in parentheses corresponds to the event number listed in Table 4.

days, the last of a series of 7 debris-flow events took place after 167 mm of rainfall (Figure 6b). Hillslope volumetric water content during this event was elevated ($\theta_p = 0.22$), but less than field saturation ($\theta_s \sim 0.4$). In fact, none of the hillslope θ measurements ever reached field saturation.

[41] Representative examples of pore fluid pressure measurements are shown in Figure 7. The pressure response differed depending on whether the sensor was buried beneath bed sediment or exposed to the flow. When exposed to the flow, the pressure transducer often recorded excess pore fluid pressures (pressures greater than hydrostatic) during debris-flow events (e.g., Figures 7b and 7c). Such high pore fluid pressures greatly contribute to the mobility of debris flows [*Iverson*, 1997; *Major and Iverson*, 1999], and have been measured previously in a large-scale flume [*Iverson et al.*, 2010] and in unburned field sites [*Berti et al.*, 2000; *McArdell et al.*, 2007; *McCoy et al.*, 2010]. Sometimes, however, anomalous pressure readings were recorded by pressure transducers exposed to the flow. This situation occurred in the middle of event 9 at Dunsmore 1 (Figure 7b). At about 00:58, the pressure dropped unexpectedly during the passage of the tail of the debris flow. Such anomalous readings are likely due to sediment clogging the sensor orifice. When the pressure transducer was buried beneath a layer of partially saturated bed sediment, the pressure signal usually tracked the stage series, but the response was damped due to unsaturated pore spaces. This type of response often occurred at Arroyo Seco as shown in Figure 7a, where the pre-event water table was approximately 4 cm below the bed surface. Similar pressure responses in unsaturated bed sediment have been observed by *McCoy et al.* [2010] and *Berger et al.* [2011]. A more detailed discussion of the pore pressure measurements at Arroyo Seco is given by *Kean and Staley* [2011].

4.3. Debris-Flow Timing

[42] The most consistent feature of the plots in Figure 6 (and the complete set in Figure S2) is the close temporal relation between stage and short-duration rainfall intensity. A quantitative measure of the temporal relation between

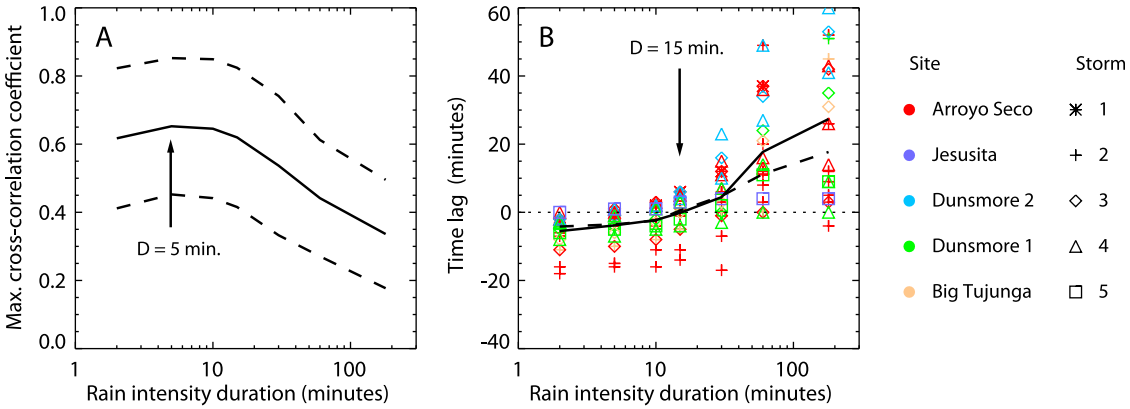

Figure 8. Comparison of debris-flow timing of 24 events relative to rainfall intensity. (a) Maximum cross-correlation coefficient ($(C_{xy})_{max}$) between stage and rainfall intensity (I_D) as a function of the duration (D) over which rainfall intensity was computed. The mean of all 24 events is shown with the solid line; ± one standard deviation is shown with the dashed line. (b) Corresponding time lag (t_{lag}) at $(C_{xy})_{max}$ between I_D and stage. A negative time lag means the peak I_D preceded the debris flow; a positive time lag means most intense rainfall came after the flow. The time lag for each event is shown with a color-coded symbol representing the site and storm. The mean time lag is shown with the solid line. For comparison, the mean time difference between peak stage and the local peak in I_D is shown with the dashed line. Stage is best correlated with I_5 ($t_{lag} = -5$ min), but most closely in phase with I_{15} ($t_{lag} = 0$).

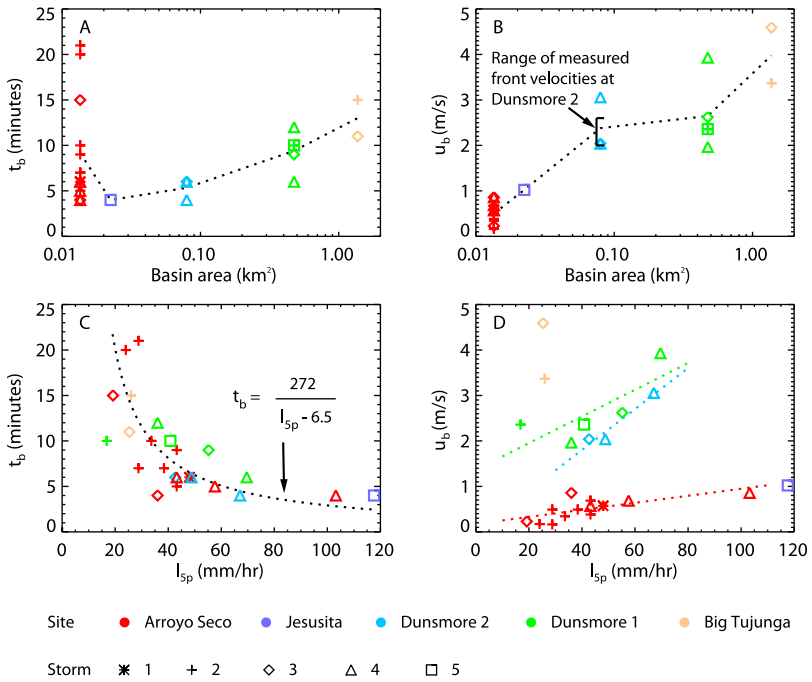

Figure 9. Comparison of basin response time (t_b) and velocity ($u_b = L_b/t_b$) scales for each event relative to (a and b) basin area and (c and d) 5-min peak rainfall intensity (I_{5p}). The mean trends with basin area are shown with the dotted lines in Figures 9a and 9b. With the exception of the smallest site, t_b increases with basin area. The velocity scale also tends to increase with basin area. Basin response times tend to decrease with increases in I_{5p} as shown by the black dotted line in Figure 9c. The form of the regression equation implies u_b should increase linearly with I_{5p}, and this trend is confirmed at three of the five sites, as shown by the dotted regression lines in Figure 9d. For reference, the range of debris-flow front velocities (2.0 to 2.6 m/s) measured at Dunsmore 2 on 18 January 2010 with spatially referenced video is shown by the black bracket in Figure 9b. Note these velocities compare favorably with the value of u_b for that event (blue diamond), and this similarity provides support for use of u_b as a velocity scale for computing the volume index.

stage and rainfall intensity for different durations is shown in Figure 8. This figure shows the maximum average stage-rainfall intensity cross-correlation coefficient ($(C_{xy})_{max}$) (Figure 8a) and the corresponding time lags (t_{lag}) between I_D and stage at this maximum (Figure 8b). A negative time lag means the peak I_D preceded the debris flow; a positive time lag means most intense rainfall came after the flow. The correlation is greatest for short durations ($D <= 30$ min) reaching a maximum at 5 min. The corresponding time lags for these durations are tightly clustered within a sub-hour range. Some of the variability within this narrow range may be related to unmeasured spatial non-uniformity in rainfall in each basin. Additional variability is related to basin size and rainfall intensity, as discussed below.

[43] The 15-min duration timescale is significant, because it is the duration where the average trend in t_{lag} goes from negative to positive (Figure 8b, solid line). In other words, at $D = 15$ min, stage and I_D are, on average, almost completely in phase ($t_{lag} = 0$). Peak rainfall intensities measured for durations shorter than 15 min generally precede the event, whereas peak rainfall intensities measured at durations longer than 15 min generally come after the peak flow. This result has major implications for debris-flow warning and is discussed in section 5. For comparison with the average trend in t_{lag}, Figure 8b also shows the average time difference between the peak stage and peak I_D (dashed line). The latter measure of flow timing relative to rainfall is more variable than the cross-correlation time lag; however, the average trend in the two is quite similar. The peak stage for all 24 events occurred within ± 25 min of the local peak in I_{15}, and for 79% of the events this time difference was within ± 10 min.

[44] Both basin area and rainfall intensity affect the timing of debris flows. Figure 9 shows trends in the basin response time and velocity scales (t_b and u_b) with respect to basin area (A_b) and event peak 5-min rainfall intensity (I_{5p}). Recall t_b is a measure of the time between the start of intense rainfall and a debris flow at the station, and u_b (L_b/t_b) is a measure of the average travel velocity of the flow through the basin. With the exception of the smallest site (Arroyo Seco), t_b follows an increasing trend with basin area, as shown by the dotted line in Figure 9a. The velocity u_b also tends to increase with basin area (Figure 9b). The Arroyo Seco site has a much wider range of response times than the other sites. Events with long response times at this site ($t_b >$ 8 min) are associated with relatively low rainfall intensities. While it is possible these events simply initiated later in the storm than other events at the site, we suspect it is more likely these debris flows began with intense rainfall but traveled very slowly as a result of insufficient fluid to overcome the flow resistance of the granular fronts. The existence of highly resistive, slow moving debris flows at

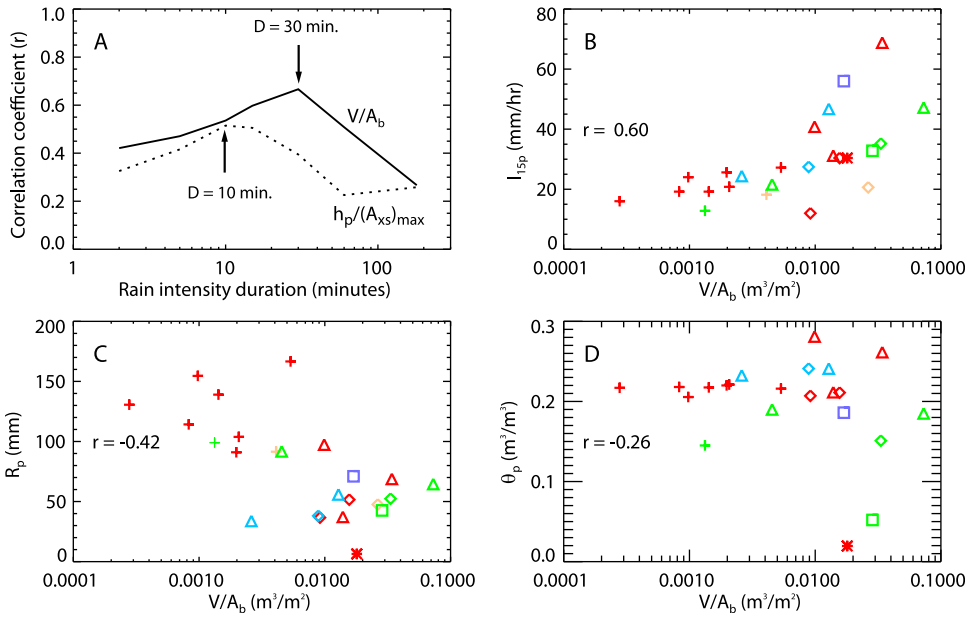

Figure 10. Comparison of debris-flow magnitude of 24 events relative to rainfall intensity, cumulative rainfall, and hillslope water content. (a) Correlations (r) between local peaks in rainfall intensity measured over different durations and both the event volume index (V, solid line) and peak flow depth (h_p, dashed line). The volume index is normalized by basin area (A_b). Peak flow depth is normalized by maximum observed flow-cross-sectional area ($(A_{xs})_{max}$). The normalized volume index is best correlated with the 15 and 30 min durations, whereas $h_p/(A_{xs})_{max}$ is best correlated with the 10-min duration. (b–d) Scatterplots of V/A_b relative to the peak 15-min rainfall intensity for the event (I_{15p}), and the cumulative rainfall and hillslope water content at the time of peak flow (R_p, and θ_p). Debris-flow magnitude is reasonably correlated with I_{15p}, but poorly correlated with R_p and θ_p. The color coded symbols represent the site and storm as described in Figure 9.

the site is supported by field observations of *Schmidt et al.* [2011]. After the first 12 November 2009 storm, they observed terminal snouts of several small debris flows deposited on the 30–35 degree hillslopes upstream of the Arroyo Seco stage gage.

[45] Figure 9c shows that basins respond more rapidly to higher intensity rainfall. This trend reflects both the control of the water/sediment concentrations on debris-flow dynamics and the scaling of flow velocity with discharge. Although it is not surprising that more intense rainfall decreases the response time, the trend in the data for the 24 events is remarkably consistent. The trend is described by the regression equation $t_b = 272/(I_{5p} - 6.5)$. This equation implies a linear dependence of u_b on rainfall intensity ($u_b = (I_{5p} - 6.5)\ L_b/272$). Linearity is evident at the three sites having more than two events, as shown by the regression lines in Figure 9d. For comparison, water flow velocity at a cross section at the outlet of a hypothetical concrete catchment under constant rainfall (i.e., no infiltration or erosion) scales similarly with rainfall intensity: $u_{xs} = Q/A_{xs} = (I\ A_b)/A_{xs}$, where Q and I are the steady discharge and rainfall intensity.

[46] While the velocity, u_b, is not a direct measure of flow velocity, its range of values is similar in magnitude to expected debris-flow velocities. At Dunsmore 2, it is possible to compare u_b to measured debris-flow front velocities at the station. As seen in Figure 9b, the value of u_b for the 18 January 2010 debris flow at Dunsmore 2 (storm 3), is within the range of front velocities measured by the video camera during the event. This similarity provides support for using u_b as a velocity scale in the volume index (equation (2)).

4.4. Debris-Flow Magnitude

[47] In this section we examine the question: How does rainfall intensity, storm cumulative rainfall, and hillslope soil water content affect debris-flow magnitude? A comparison of the volume index (V) and peak flow depth (h_p) of the events relative to I_D, R, and θ is shown in Figure 10. The volume index is normalized by basin area (A_b) in order facilitate comparison between sites that span two orders of magnitude in size. Similarly, peak flow depth is normalized by the maximum flow cross-sectional area observed at the station ($(A_{xs})_{max}$). This area is approximately the area between the red cross section and blue flow surface shown in Figure 4. As with debris-flow timing, it is instructive to first see how V and h_p correlate with rainfall intensity measured over different durations (Figure 10a). Both variables are best correlated with short duration ($D <= 30$ min) rainfall intensity. The normalized peak depth is best correlated with I_{10} ($r = 0.51$), whereas the normalized volume index is better correlated with the slightly longer durations of 15 min ($r = 0.60$) and 30 min ($r = 0.67$). While debris-flow volume and peak depth are related, the slight differences in the correlations of these variables with rainfall intensity suggest these two variables are at least partially controlled by different rainfall characteristics. A possible explanation is that a burst of high intensity rainfall could generate enough runoff to trigger a relatively large ampli-

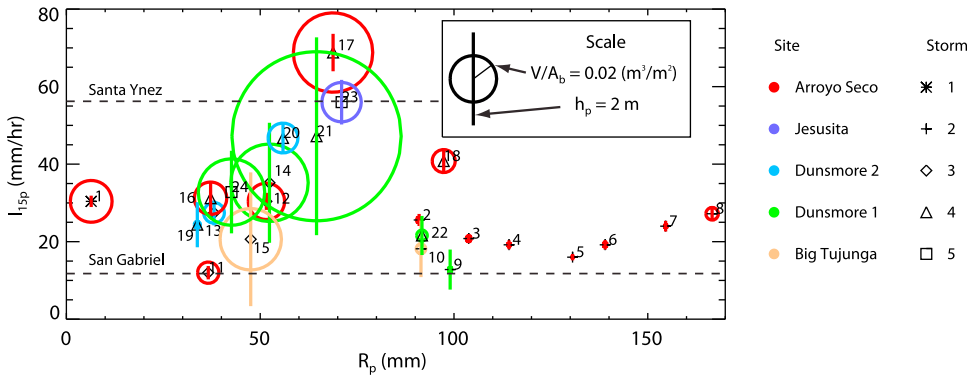

Figure 11. Overview of V and h_p relative to I_{15p} and R_p. The radius of each circle is scaled by the V/A_b. The vertical lines are scaled by the measured peak flow depth (h_p). The numbers in the figure correspond to the event numbers listed in Table 4. The approximate rainfall intensity thresholds for debris flows in the San Gabriel and Santa Ynez Mountains are shown with the horizontal dotted lines.

tude debris-flow surge, but without sustained high-intensity rainfall, the volume of this event may be small.

[48] The three scatterplots in Figures 10b–10d show that the normalized volume index (V/A_b) is reasonably correlated with peak 15-min rainfall intensity (I_{15p}), but poorly correlated with both storm cumulative rainfall (R_p) and hillsope soil water content (θ_p) at the time of peak flow. The trends of R_p and θ_p with respect to peak depth (not shown) are similarly poor. While it is intuitive that debris-flow magnitude should increase with rainfall intensity, the observed lack of a correlation between the volume index and both R_p and θ_p was not entirely expected. On one hand, field observations of debris flows by *Coe et al.* [2008] at Chalk Cliffs, Colorado have shown that, given sufficient rainfall intensity, debris flows can occur after very little cumulative rainfall when the hillslope soil is relatively dry. Event 1 from our data set (red asterisk, Figures 10c and 10d) is another example of this situation. On the other hand, however, recent work by *Iverson et al.* [2011] demonstrated that debris-flow volume (and momentum) in a large-scale flume increased dramatically as the bed water content increased above a value of 0.22. The increase in volume was shown to be caused by the development of positive pore pressures in wet bed sediments by the overriding debris flow, which promoted progressive bed scour and reduced basal friction. They suggested that bed sediment with water contents below 0.22 could not transmit the destabilizing positive pore fluid pressures into the bed, because the pore fluid was disconnected by air bubbles. Although we did not measure bed soil water content, one might expect it would increase as hillslope soil water content and storm cumulative rainfall also increased.

[49] We hypothesize that the discrepancy between the findings of *Iverson et al.* [2011] and our observed lack of relation between the volume index and both R and hillslope θ may be because the bed sediment at our sites was sufficiently porous that it drained to relatively low water contents in between rainfall bursts. This hypothesis is partially supported by our measurements of channel bed pore fluid pressure accompanying the series of 7 events during the 12–13 December 2009 storm at Arroyo Seco. These 7 events each had similar small volume indexes, despite a relatively broad range in storm cumulative rainfall from 91 mm to 167 mm (hillslope θ_p was consistent for these events at about 0.22). Although the bed pore fluid pressure (and water table) rose in response to each rainfall burst and flow event, it dropped to unsaturated levels before the next event began. Hillslope water content also dropped rapidly after each rain burst. This cycle continued even after 167 mm of storm cumulative rainfall, which fell prior to the last event of the storm (Figure 7a; see also *Kean and Staley* [2011] for a complete time series of the pore fluid pressure at Arroyo Seco). Had the rain bursts come in faster succession, and the bed had less time to drain between bursts, there likely would have been a systematic increase in the bed water content and event volume throughout the storm.

[50] An alternative way to visualize the interrelations between V, h_p, I_{15p} and R_p is given in Figure 11. This figure illustrates two important aspects of the data regarding sediment supply and geologic material. The vertical lines for each event represent h_p; the radius of the circle for an event is scaled by V/A_b. For many events V/A_b is too small to see a circle. In regards to sediment supply, some of the largest debris flows at the sites occurred toward the end of the winter storm season (e.g., 17, 20, 21, and 23) and, in most cases, after multiple debris-flow events had already taken place. The late season timing of the large events is opposite of the trend observed after other southern California fires [e.g., *Wells*, 1987]; however, it is largely due to the fact that the late winter storms happened to have the most intense rainfall. The fact that these late season events were still large, despite substantial erosion from previous events, provides yet another example of the tremendous amount sediment available for transport after wildfire [e.g., *Doehring*, 1968; *Wells*, 1985; *Moody and Martin*, 2001b]. Although, there is some evidence that the smallest site (Arroyo Seco) was reaching supply limited conditions toward the end of the season as mentioned in section 4.2, supply limited conditions were not reached in the larger basins. For example at Dunsmore 1, despite following four debris flows at the site earlier that winter, event 24 on 27 February 2010 (the last storm of the season) produced long, well-developed debris-flow levees indicating the flow had a high volume fraction of solids. The contrast in late season sediment supply between the small Arroyo Seco site and the

much larger Dunsmore 1 site suggests that flows early in the season drew sediment primarily from dry ravel loaded channels and hillslopes, whereas subsequent flows drew more sediment from erosion of older bed and bank material. This trend is also supported by the observed shift in erosion characteristics and deposit grain size distribution between the first and second event at Big Tujunga, as discussed in section 4.2.

[51] Regarding geologic materials, Figure 11 shows an important difference between the debris flows recorded in the San Gabriel Mountains (granitic bedrock) and the Santa Ynez Mountains (sandstone bedrock). Although the debris flows in both areas occurred in response to short duration bursts of rainfall resulting in similar hillslope and channel erosion characteristics, there is a substantial difference in the threshold triggering rainfall intensity for the two areas. The lowest peak rainfall intensity associated with a debris flow in the San Gabriel sites was I_{15p} = 12 mm/hr (event 11, Arroyo Seco), whereas the peak rainfall intensity accompanying the only debris flow recorded at the Santa Ynez site on 27 February 2010 was I_{15p} = 56 mm/hr (event 23, Jesusita). The second highest rainfall intensity measured at Jesusita was I_{15p} = 40 mm/hr and resulted in a minor 15 cm deep water flood. Storms of lesser rainfall intensity at Jesusita resulted in negligible flow. The measurements at Jesusita, which are consistent with the observed flow response elsewhere in the burned area, constrain the 15-min rainfall intensity threshold for the Santa Ynez Mountains to be between 40 and 56 mm/hr, which is about 4 times higher than the San Gabriel Mountain threshold.

[52] Unfortunately, our measurements do not clearly identify the physical reason for the different rainfall intensity thresholds between the San Gabriel and Santa Ynez Mountains. One simple explanation for the higher debris-flow threshold at Jesusita could be that the site is slightly less steep than the San Gabriel sites (see Table 1). This explanation, however, is unlikely to be the reason for the difference in thresholds, because the surrounding burn area in the Santa Ynez Mountains, which included basins as steep as the San Gabriel sites, only produced debris flows during the 27 February 2010 storm. A second explanation could be related to differences in the effective infiltration rates between the two areas, which control the rainfall intensity required to produce overland flow. The effective infiltration is controlled by a number of factors including: extent of exposed rock, depth to bedrock, and spatial and temporal variability in local infiltration rates, which are influenced by soil composition, and fire-related ash content and water repellency [e.g., *Shakesby and Doerr*, 2006; *Kinner and Moody*, 2010]. Although the effective infiltration rate for a burned basin is particularly difficult to characterize, our field observations do not suggest there is a substantial difference in this property between the San Gabriel sites and the Santa Ynez site, because both areas are predominately soil mantled, and measurements of local infiltration rates were similar. A third explanation could be related to sediment transport and the grain-size distribution of sediments at the study sites. The grain size distribution of the hillslope sediment is the only basin characteristic that is substantially different between the two areas (Table 2), and the Jesusita hillslope sediment contains a higher fraction of silt and clay than the San Gabriel sites. It is possible that intermediate rainfall intensities (above the San Gabriel threshold, but below the Santa Ynez threshold) do not result in debris flows in the Santa Ynez Mountains, because the sediment is sufficiently fine to be completely transported as ordinary bed and suspended load without bulking into a debris flow. Debris flows may form with the addition of larger clasts mobilized from the increased runoff generated by higher rainfall intensities. This third explanation is the most consistent with our observations; however, additional measurements and work to understand the transition of surface water flow to debris flow are needed to test this hypothesis.

4.5. Volume Index Versus True Volume

[53] Although the primary purpose of the volume index is to make relative comparisons between events in the data set, it is worthwhile to assess how the volume index compares to actual debris-flow volumes. A crude comparison is possible for the 6 February 2010 storm using volume data from a Los Angeles County debris basin (Dunsmuir debris basin) that is located downstream of both Dunsmore 1 and Dunsmore 2. This storm conveniently filled the previously empty debris basin to capacity (95000 m^3). To make a comparison with the volume indexes from Dunsmore 1 and Dunsmore 2, which represent a fraction of the total drainage area of the Dunsmuir debris basin, we weight the debris basin capacity by the percent of area that was monitored (27%). The total of the volume indexes of the 4 events recorded at Dunsmore 1 and Dunsmore 2 during the 6 February 2010 storm (events 19–22) is 38000 m^3. This volume is 1.5 times greater than the area-weighted volume of the debris basin (26000 m^3). Based on this comparison, we conclude the volume index is at least the same order of magnitude as a conventional volume estimate from a debris basin, and may be a conservative over estimate of actual debris-flow volume.

4.6. Slope Stability

[54] Results from slope stability calculations for a representative section of Arroyo Seco hillsope provide insight into why meter-scale shallow landslides were not widely observed and estimate the conditions in which they might be expected. The measured parameters for this hillslope were, α = 40°, $d_{LZ} = 0.8/\cos(\alpha)$ = 1.04 m, c = 9600 Pa, ϕ = 41°, γ_s = 19000 kg/m^3, γ_w = 9800 kg/m^3, and K_s = 0.0002 m/s. We estimated the specific storage and *Gardner*'s [1958] soil-water characteristic curve parameter to be 0.1 m^{-1} and 5.4 m^{-1}, respectively, based on soils with the same textural classification. Under conditions of complete saturation ($\psi = Z\cos^2\alpha$) and assuming no additional strength from root cohesion, equation (3) shows the slope is stable to a vertical depth of 2.05 m. This depth is almost twice the observed depths to bedrock $d_{LZ} \leq 1$ m. Equation (3) shows that failure at Z = 1 m could occur for a saturated slope having slightly less than half of the measured soil cohesion (c = 4700 Pa).

[55] The model TRIGRS [*Baum et al.*, 2008, 2010] was used to investigate if the most intense storm of the monitoring period (6 February 2010) was sufficient to saturate and destabilize this slope with lower cohesion. At Arroyo Seco, this storm had three major peaks in rainfall intensity, which each produced debris flows (events 16, 17, 18; I_{5p} = 43, 103, and 58 mm/hr; R_p = 37, 69, and 97 mm; t_p = 17, 19,

and 21 h). Like the other storms, this storm began with relatively dry initial conditions (θ_r = 0.1), and there was no pre-existing hillslope water table. TRIGRS computes ψ (Z,t) relative to an initial water table, and we assumed this to be at the bedrock surface to provide a lower bound on time to failure. Using this assumption and neglecting near-surface hydrophobic layers, which would limit infiltration and delay time to failure, the modeled slope remained unsaturated and the lowest factor of safety calculated during the storm was 1.5.

[56] For comparison, we examined two other scenarios where landslide failure would occur: (1) a slope with soils of zero cohesion and (2) a slope with soils having modest cohesion (c = 1000 Pa) during a hypothetical storm with twice the measured rainfall intensity. In the first case, the matric suction in the unsaturated zone is sufficient to keep the cohesionless slope stable until the time of the second rain burst and debris flow. In the second case, failure would occur 19 min after the second recorded debris flow, which is almost four times longer than the observed timescale of response. Based on these calculations, shallow landslides would be expected for conditions of much less cohesion and/or greater rainfall than measured.

5. Discussion

[57] The results from our post-fire debris flow monitoring stations have important implications for debris-flow warning and prediction. The observed rapid debris-flow response to rainfall means that real-time data from monitoring stations in burn areas cannot provide sufficient warning of impending debris flows for communities downstream. Instead, warnings with practical lead times of hours must come from weather forecasts, real-time rainfall measurements of advancing storms before they impact burned areas, and debris-flow thresholds, such as the regional thresholds of *Cannon et al.* [2011]. Thus, advancement in post-fire debris-flow warning rests largely on improving short-duration high-intensity rainfall prediction and specification of more precise rainfall thresholds. Forecasting the location and magnitude of high intensity rainfall is among the most challenging problems in weather prediction; however, advanced radar technologies, such as portable dual-polarized radar, show promise in helping to better identify localized high intensity cells [*Jorgensen et al.*, 2011]. In areas of southern California with relatively limited data, such as the Santa Ynez Mountains, more precise empirical rainfall thresholds can be developed with additional basic data on rainfall and debris-flow occurrence. However, in better studied areas, such as the San Gabriel Mountains, collection of additional data will not likely result in major improvements to the regional thresholds. Improvements in these areas will require development of more refined basin specific thresholds.

[58] Detailed data, such as that presented here, provides valuable constraints for development of physically based models of post-fire debris flows, which may aid in the specification of basin specific rainfall thresholds. The high correlation between short-duration high-intensity rainfall and debris flows suggests that a simple rainfall-runoff model [e.g., *Berti and Simoni*, 2005; *Coe et al.*, 2008; *Gregoretti and Fontana*, 2008] may be a useful tool to help predict the timing of post-fire debris-flows. However, without the addition of debris-flow mechanics for initiation, entrainment [*Iverson et al.*, 2011] and flow dynamics [e.g., *Iverson and Denlinger*, 2001; *Denlinger and Iverson*, 2001], rainfall-runoff models will not reproduce the complex stage changes of the debris-flow surges shown in Figure 6, nor predict accurately the volume or peak stage of debris flows, which can be much higher than flood peaks [*VanDine*, 1985]. A particular challenge for prediction is that the water/sediment mixture concentrations, which control the flow dynamics, can vary considerably during an event and over the course of the storm season.

[59] Further attention needs to be given to the mechanics by which post-fire debris flows initiate in order to better understand why the rainfall thresholds vary for different regions. Although field observations of erosion features, slope stability modeling, and the observed time scale for debris-flow response all suggest that the recorded events were initiated primarily by surface water flow rather than by failure of discrete meter-scale landslides, our measurements do not identify the mechanics by which the transition of surface water to debris flow takes place. Such a transition may occur by several mechanisms including the "firehose effect" [*Johnson and Rodine*, 1984], failure of the channel bed by sliding [*Takahashi*, 1981] or hydrodynamic forces [*Tognacca et al.*, 2000; *Armanini and Gregoretti*, 2000], sediment bulking from erosion of bank material, and formation and failure of sediment dams created by local deposition of bed load. It is possible that several of these mechanisms operate during a single event. Additional observations using a series of stations and cameras that bracket the transition of surface water flow to debris flow could provide valuable constraints on the mechanics by which this transformation occurs.

6. Summary and Conclusions

[60] Using direct measurements of rainfall, flow stage, hillslope soil water content and channel bed pore fluid pressure at five sites, this study identified the hydrologic triggering conditions associated with 24 post-fire debris flows in southern California. The data show that both the timing and magnitude of the recorded debris flows were controlled consistently by short duration (< = 30 min), high intensity rainfall. These results confirm our hypothesis that, in the first year after the fire, the timing of post-fire debris flows is consistently tied to the onset of high intensity rainfall capable of producing overland flow. Storm cumulative rainfall and hillslope soil water content, two other variables we suspected could influence debris-flow magnitude, were found to be poorly correlated with an index of debris-flow volume. The lack of correlation may be because the rainfall intensities prior to triggering rain bursts were too low to sustain high water contents in the relatively porous hillslope soil and bed material.

[61] While the temporal coincidence of the debris flows with high intensity rainfall is remarkably consistent across sites of different size and geologic material, distinct differences in the flow dynamics were observed during the winter storm season. At the smallest site (0.014 km^2), a decrease in the hillslope and channel sediment supply over the winter likely caused a shift in flow dynamics from multiple surges

in the first half of the season to single surge flows having higher volume fractions of water than the earlier flows. The larger sites were not supply limited; however there is some evidence for a shift in source material over the winter, from finer material eroded from the hillslopes and ravel loaded channels early in the season, to coarse material eroded from older bed and bank deposits later in the season. At the largest site (1.4 km^2), the addition of coarse material from erosion of the bed and banks during the second event at the site likely caused the almost tripling of peak stage from that of the first storm, which had comparable rainfall intensity.

[62] The most important aspects of this study for post-fire debris-flow warning and prediction are that it (1) identified the rainfall characteristics that deserve the most attention for monitoring and forecasting, (2) showed the timescale for post-fire debris-flow generation is exceedingly short (minutes), so warning must come before a storm is over a burn area, and (3) showed that the potential for dangerous debris flows does not diminish after one or more debris flows have occurred. Although post-fire debris-flow monitoring is not practical for providing advanced warning because of the short timescale of response, it is invaluable for providing the constraints necessary to advance physical understanding of debris flows. This first set of direct measurements of post-fire debris flows represents an important step in this direction; however additional work is needed. Our measurements have helped frame an important next question: What are the dominant mechanics controlling the transition of surface-water flow to debris flow in a burn area, and how do these do these mechanics control the threshold for debris-flow initiation? Definitively answering this question will likely require additional direct measurements of post-fire runoff in future burn areas.

Notation

A_b basin area above station, L^2.
A_{xs} flow cross-sectional area at station, L^2.
$(A_{xs})_{\max}$ maximum flow cross-sectional area observed at station, L^2.
$(\overline{A_{xs}})_{post}$ summation of flow cross-sectional area after peak flow, L^2T.
c soil cohesion, $M/(LT^2)$.
C_{xy} cross-correlation coefficient between stage and rainfall intensity for a given time lag, dimensionless.
$(C_{xy})_{\max}$ maximum cross-correlation coefficient, dimensionless.
D rainfall duration, T.
d_Z vertical depth to bedrock on a hillslope, L.
Fs factor of safety, dimensionless.
H flow stage time series, L.
H_p event peak flow stage, L.
h_p event peak flow depth, L.
I_D rainfall intensity for a given duration, L/T.
I_5 5-min rainfall intensity time series, L/T.
I_{5p} event peak 5-min rainfall intensity, L/T.
I_{15} 15-min rainfall intensity time series, L/T.
I_{15p} event peak 15-min rainfall intensity, L/T.
K_s saturated hydraulic conductivity, L/T.
l cross-correlation time lag, T.
L_b length of basin along main channel from outlet to drainage divide, L.
P channel bed pore fluid pressure head, L.
r correlation coefficient, dimensionless.
R storm cumulative rainfall time series, L.
R_p storm cumulative rainfall at time of peak flow, L.
t time, T.
t_b time scale for basin response, T.
t_{lag} time lag corresponding to the maximum stage-rainfall intensity cross-correlation coefficient, T.
t_p elapsed time from start of storm to peak flow, T.
u_b basin travel velocity scale used in computing the volume index, L/T.
u_{xs} flow velocity at station cross section, L/T.
V volume index, L^3.
Z vertical coordinate direction (positive downward), L.
α slope angle, dimensionless.
γ_s unit weight of soil, M/L^2T^2.
γ_w unit weight of water, M/L^2T^2.
θ volumetric soil water content time series, dimensionless.
θ_p event peak volumetric soil water content, dimensionless.
θ_r pre-storm residual soil water content, dimensionless.
θ_s soil water content at saturation, dimensionless.
ϕ soil friction angle, dimensionless.
ψ groundwater pressure head, L.

[63] **Acknowledgments.** We thank Robert Leeper, Kevin Schmidt, Joseph Gartner, Yonni Schwartz, and Lucy Jones for field and logistical support; Daniel Meisel, James Marquiss, and the cities of Glendale and Pasadena for land access; L.A. County Fire Department for the helicopter ride; the National Center for Airborne Laser Mapping for Station Fire topographic data; Jeffrey Coe, Scott McCoy, and Jonathan Stock for helpful comments on an earlier version of this manuscript; and Leslie Hsu, Brian McArdell, Paul Santi, and the Associate Editor, Jon Major, for constructive comments on this manuscript.

References

Arattano, M., and L. Marchi (2000), Video-derived velocity distribution along a debris flow surge, *Phys. Chem. Earth, Part B*, *25*(9), 781–784, doi:10.1016/S1464-1909(00)00101-5.

Armanini, A., and C. Gregoretti (2000), Triggering of debris flow by overland flow: A comparison between theoretical and experimental results, in *Proceedings of the 2nd International Conference on Debris Flow Hazards Mitigation*, edited by G. F. Wieczorek and N. D. Naeser, pp. 117–124, A. A. Balkema, Rotterdam, Netherlands.

Baum, R. L., and J. W. Godt (2010), Early warning of rainfall-induced shallow landslides and debris flows in the USA, *Landslides*, *7*, 259–272, doi:101007/s10346–009–0177–0.

Baum, R. L., W. Z. Savage, and J. W. Godt (2008), TRIGRS—A FORTRAN program for transient rainfall infiltration and grid-based regional slope-stability analysis, version 2.0, *U.S. Geol. Surv Open File Rep. 2008-1159*, 74 pp.

Baum, R. L., J. W. Godt, and W. Z. Savage (2010), Estimating the timing and location of shallow rainfall-induced landslides using a model for transient, unsaturated infiltration, *J. Geophys. Res.*, *115*, F03013, doi:10.1029/2009JF001321.

Berger, C., B. W. McArdell, B. Fritschi, and F. Schlunegger (2010), A novel method for measuring the timing of bed erosion during debris flows and floods, *Water Resour. Res.*, *46*, W02502, doi:10.1029/2009WR007993.

Berger, C., B. W. McArdell, and F. Schlunegger (2011), Direct measurement of channel erosion by debris flows, Illgraben, Switzerland, *J. Geophys. Res.*, *116*, F01002, doi:10.1029/2010JF001722.

Berti, M., and A. Simoni (2005), Experimental evidences and numerical modelling of debris flow initiated by channel runoff, *Landslides*, *2*, 171–182, doi:10.1007/s10346-005-0062-4.

Berti, M., R. Genovois, A. Simoni, and P. R. Tecca (1999), Field observations of a debris flow event in the Dolomites, *Geomorphology*, *29*, 265–274, doi:10.1016/S0169-555X(99)00018-5.

Berti, M., R. Genevois, R. LaHusen, A. Simoni, and P. R. Tecca (2000), Debris flow monitoring in the acquabona watershed in the Dolomites (Italian Alps), *Phys. Chem. Earth, Part B*, *25*(9), 707–715, doi:10.1016/S1464-1909(00)00090-3.

Caine, N. (1980), The rainfall intensity-duration control of shallow landslides and debris flows, *Geogr. Ann., Ser. A*, *62*, 23–27.

Cannon, S. H., R. M. Kirkham, and M. Parise (2001), Wildfire-related debris-flow initiation processes, Storm King Mountain, Colorado, *Geomorphology*, *39*, 171–188, doi:10.1016/S0169-555X(00)00108-2.

Cannon, S. H., J. E. Gartner, R. C. Wilson, J. C. Bowers, and J. L. Laber (2008), Storm rainfall conditions for floods and debris flows from recently burned areas in southwestern Colorado and southern California, *Geomorphology*, *96*, 250–269, doi:10.1016/j.geomorph.2007.03.019.

Cannon, S. H., E. M. Boldt, J. L. Laber, J. W. Kean, and D. M. Staley (2011), Rainfall intensity-duration thresholds for postfire debris-flow emergency-response planning, *Nat. Hazards*, *59*, 209–236, doi:10.1007/s11069-011-9747-2.

Chawner, W. D. (1934), The Montrose–La Crescenta (California) flood of 1 January 1934, and its sedimentary aspects, M.S. thesis, Calif. Inst. of Technol., Pasadena.

Chong, J., J. Renaud, and E. Ailsworth (2004), Flash floods wash away lives, dreams, *Los Angeles Times*, p. B.1, 3 Jan.

Coe, J. A., D. A. Kinner, and J. W. Godt (2008), Initiation conditions for debris flows generated by runoff at Chalk Cliffs, central Colorado, *Geomorphology*, *96*, 270–297, doi:10.1016/j.geomorph.2007.03.017.

Denlinger, R. P., and R. M. Iverson (2001), Flow of variably fluidized granular masses across three-dimensional terrain: 2. Numerical predictions and experimental tests, *J. Geophys. Res.*, *106*, 553–566, doi:10.1029/2000JB900330.

Doehring, D. O. (1968), The effect of fire on geomorphic process in the San Gabriel Mountains, California, *Contrib. Geol.*, *7*, 43–65.

Eaton, E. C. (1935), Flood and erosion control problems and their solution, *Proc. Am. Soc. Civ. Eng.*, *62*(8), 1302–1362.

Florsheim, J. L., E. A. Keller, and D. W. Best (1991), Fluvial sediment transport in response to moderate storm flows following chaparral wildfire, Ventura County, southern California, *Geol. Soc. Am. Bull.*, *103*, 504–511, doi:10.1130/0016-7606(1991)103<0504:FSTIRT>2.3.CO;2.

Gabet, E. J. (2003), Post-fire thin debris flow: Sediment transport and numerical modelling, *Earth Surf. Processes Landforms*, *28*, 1341–1348, doi:10.1002/esp.590.

Gabet, E. J., and A. Bookter (2008), A morphometric analysis of gullies scoured by post-fire progressively bulked debris flows in southwest Montana, USA, *Geomorphology*, *96*, 298–309, doi:10.1016/j.geomorph.2007.03.016.

Gardner, W. R. (1958), Some steady-state solutions of the unsaturated moisture flow equation with application to evaporation from a water table, *Soil Sci.*, *85*, 228–232, doi:10.1097/00010694-195804000-00006.

Gartner, J. E., S. H. Cannon, P. M. Santi, and V. G. DeWolfe (2008), Empirical models to predict the volumes of debris flows generated by recently burned basins in the western U.S, *Geomorphology*, *96*, 339–354, doi:10.1016/j.geomorph.2007.02.033.

Gregoretti, C., and G. D. Fontana (2008), The triggering of debris flow due to channel-bed failure in some alpine headwater basins of the Dolomites: Analyses of critical runoff, *Hydrol. Processes*, *22*, 2248–2263, doi:10.1002/hyp.6821.

Guzzetti, F., S. Peruccacci, M. Rossi, and C. P. Stark (2008), The rainfall intensity-duration control of shallow landslides and debris flows: An update, *Landslides*, *5*, 3–17, doi:10.1007/s10346-007-0112-1.

Hungr, O. (2000), Analysis of debris flow surges using the theory of uniformly progressive flow, *Earth Surf. Processes Landforms*, *25*, 483–495, doi:10.1002/(SICI)1096-9837(200005)25:5<483::AID-ESP76>3.0.CO;2-Z.

Hürlimann, M., D. Rickenmann, and C. Graf (2003), Field and monitoring data of debris-flow events in the Swiss Alps, *Can. Geotech. J.*, *40*, 161–175, doi:10.1139/t02-087.

Iverson, R. M. (1997), The physics of debris flow, *Rev. Geophys.*, *35*, 245–296, doi:10.1029/97RG00426.

Iverson, R. M. (2000), Landslide triggering by rain infiltration, *Water Resour. Res.*, *36*, 1897–1910, doi:10.1029/2000WR900090.

Iverson, R. M., and R. P. Denlinger (2001), Flow of variably fluidized granular masses across three-dimensional terrain: 1. Coulomb mixture theory, *J. Geophys. Res.*, *106*, 537–552, doi:10.1029/2000JB900329.

Iverson, R. M., S. P. Schilling, and J. W. Vallance (1998), Objective delineation of lahar-inundation hazard zones, *Geol. Soc. Am. Bull.*, *110*(8), 972–984, doi:10.1130/0016-7606(1998)110<0972:ODOLIH>2.3.CO;2.

Iverson, R. M., M. Logan, R. G. LaHusen, and M. Berti (2010), The perfect debris flow? Aggregated results from 28 large-scale experiments, *J. Geophys. Res.*, *115*, F03005, doi:10.1029/2009JF001514.

Iverson, R. M., M. E. Reid, M. Logan, R. G. LaHusen, J. W. Godt, and J. P. Griswold (2011), Positive feedback and momentum growth during debris-flow entrainment of wet bed sediment, *Nat. Geosci.*, *4*, 116–121, doi:10.1038/ngeo1040.

Johnson, A. M., and J. R. Rodine (1984), Debris flow, in *Slope Instability*, edited by D. Brunsden and D. B. Prior, pp. 257–361, John Wiley, Chichester, U. K.

Jorgensen, D. P., M. N. Hanshaw, K. M. Schmidt, J. L. Laber, D. M. Staley, J. W. Kean, and P. J. Restrepo (2011), Value of a dual-polarized gap-filling radar in support of southern California post-fire debris-flow warnings, *J. Hydrometeorol.*, doi:10.1175/JHM-D-11-05.1, in press.

Kean, J. W., and D. M. Staley (2011), Direct measurements of the hydrologic conditions leading up to and during post-fire debris flow in southern California, USA, in *Debris-Flow Hazards Mitigation, Mechanics, Prediction, and Assessment*, edited by R. Genevois, D. L. Hamilton, and A. Prestininzi, pp. 685–694, Casa Editrice Univ. La Sapienza, Rome.

Kinner, D. A., and J. A. Moody (2010), Spatial variability of steady-state infiltration into a two-layer soil system on burned hillslopes, *J. Hydrol.*, *381*, 322–332, doi:10.1016/j.jhydrol.2009.12.004.

Larsen, I. J., J. L. Pederson, and J. C. Schmidt (2006), Geologic versus wildfire controls on hillslope processes and debris flow initiation in the Green River canyons of Dinosaur National Monument, *Geomorphology*, *81*, 114–127, doi:10.1016/j.geomorph.2006.04.002.

Leeper, R. J., J. W. Kean, and D. M. Staley (2010), A low-cost method to measure the timing of post-fire debris flows and flash floods, paper presented at Annual Meeting, Geol. Soc. of Am., Denver, Colo.

Lin, R. G., V. Kim, and R. Vives (2010), 'Niagara' of mud hits homes; Dozens of houses in La Canada Flintridge are damaged or destroyed in a storm that defied forecast, *Los Angeles Times*, p. A.1, 7 Feb.

Major, J. J., and R. M. Iverson (1999), Debris-flow deposition: Effects of pore-fluid pressure and friction concentrated at flow margins, *Geol. Soc. Am. Bull.*, *111*, 1424–1434, doi:10.1130/0016-7606(1999)111<1424:DFDEOP>2.3.CO;2.

Malmon, D. V., S. L. Reneau, D. Katzmann, A. Lavine, and J. Lyman (2007), Suspended sediment transport in an ephemeral stream following wildfire, *J. Geophys. Res.*, *112*, F02006, doi:10.1029/2005JF000459.

Marchi, L., M. Arattano, and A. Deganutti (2002), Ten years of debris-flow monitoring in the Moscardo Torrent (Italian Alps), *Geomorphology*, *46*, 1–17, doi:10.1016/S0169-555X(01)00162-3.

McArdell, B. W., P. Bartelt, and J. Kowalski (2007), Field observations of basal forces and fluid pore pressure in a debris flow, *Geophys. Res. Lett.*, *34*, L07406, doi:10.1029/2006GL029183.

McCoy, S. W., J. W. Kean, J. A. Coe, D. M. Staley, T. A. Wasklewicz, and G. E. Tucker (2010), Evolution of a natural debris flow: In situ measurements of flow dynamics, video imagery, and terrestrial laser scanning, *Geology*, *38*, 735–738, doi:10.1130/G30928.1.

McCoy, S. W., J. A. Coe, J. W. Kean, G. E. Tucker, D. M. Staley, and T. A. Wasklewicz (2011), Observations of debris flows at Chalk Cliffs, Colorado, USA: Part 1, In-situ measurements of flow dynamics, tracer particle movement, and video imagery from the summer of 2009, *Ital. J. Eng. Geol. Environ.*, *1*(11), 67–75.

McPhee, J. A. (1989), *The Control of Nature*, 272 pp., Farrar, Straus and Giroux, New York.

Meyer, G. A., and S. G. Wells (1997), Fire-related sedimentation events on alluvial fans, Yellowstone National Park, U.S.A., *J. Sediment. Res.*, *67*(5), 776–791, doi:10.1306/D426863A-2B26-11D7-8648000102C1865D.

Meyer, G. A., J. L. Pierce, S. H. Wood, and A. J. T. Jull (2001), Fire, storms, and erosional events in the Idaho batholith, *Hydrol. Processes*, *15*, 3025–3038, doi:10.1002/hyp.389.

Minor, S. A., K. S. Kellogg, R. G. Stanley, L. D. Gurrola, E. A. Keller, and T. R. Brandt (2009), Geologic map of the Santa Barbara coastal plain area, Santa Barbara County, California, *U.S. Geol. Surv. Sci. Invest. Map*, *3001*, 38 pp.

Moody, J. A., and D. A. Martin (2001a), Post-fire, rainfall intensity–peak discharge relations for three mountainous watersheds in the western USA, *Hydrol. Processes*, *15*, 2981–2993, doi:10.1002/hyp.386.

Moody, J. A., and D. A. Martin (2001b), Hydrologic and sedimentologic response of two burned watersheds in Colorado, *U.S. Geol. Surv. Water Resour. Invest. Rep., 01-4122*, 138 pp.

NOAA-USGS Debris Flow Task Force (2005), NOAA-USGS debris-flow warning system—Final report, *U.S. Geol. Surv. Circ.*, *1283*, 47 pp.

Nyman, P., G. J. Sheridan, H. G. Smith, and P. N. J. Lane (2011), Evidence of debris flow occurrence after wildfire in upland catchments of south-east Australia, *Geomorphology*, *125*, 383–401, doi:10.1016/j.geomorph.2010.10.016.

Pierson, T. C. (1986), Flow behaviour of channelized debris flows, Mount St. Helens, Washington, in *Hillslope Processes*, edited by A. D. Abrahams, pp. 269–296, Allen and Unwin, Boston, Mass.

Rice, R. M., and G. T. Foggin III (1971), Effect of high intensity storms in on soil slippage on mountainous watersheds in southern California, *Water Resour. Res.*, *7*, 1485–1496, doi:10.1029/WR007i006p01485.

Santi, P. M., V. G. deWolfe, J. D. Higgins, S. H. Cannon, and J. E. Gartner (2008), Sources of debris flow material in burned areas, *Geomorphology*, *96*, 310–321, doi:10.1016/j.geomorph.2007.02.022.

Schmidt, K. M., M. N. Hanshaw, J. F. Howle, J. W. Kean, D. M. Staley, J. D. Stock, and G. W. Bawden (2011), Hydrologic conditions and terrestrial laser scanning of post-fire debris flows in the San Gabriel Mountains, CA, U.S.A., in *Debris-Flow Hazards Mitigation, Mechanics, Prediction, and Assessment*, edited by R. Genevois, D. L. Hamilton, and A. Prestininzi, pp. 583–593, Casa Editrice Univ. La Sapienza, Rome.

Scott, K. M. (1971), Origin and sedimentology of 1969 debris flows near Glendora, California, in *Geological Survey Research 1971 Chapter C*, *U.S. Geol. Surv. Prof. Pap.*, *750C*, C242–C247.

Shakesby, R. A., and S. H. Doerr (2006), Wildfire as a hydrological and geomorphological agent, *Earth Sci. Rev.*, *74*, 269–307, doi:10.1016/j.earscirev.2005.10.006.

Suwa, H., K. Okunishi, and M. Sakai (1993), Motion, debris size and scale of debris flows in a valley on Mount Yakedake, Japan, in Sediment Problems: Strategies for Monitoring, Prediction and Control, *IAHS Publ.*, *217*, 239–248.

Suwa, H., K. Okano, and T. Kanno (2009), Behavior of debris flows monitored on test slopes of Kamikamihorizawa Creek, Mount Yakedake, Japan, *Int. J. Erosion Control Eng.*, *2*, 33–45.

Takahashi, T. (1981), Debris flow, *Annu. Rev. Fluid Mech.*, *13*, 57–77, doi:10.1146/annurev.fl.13.010181.000421.

Tognacca, C., G. R. Bezzola, and H. E. Minor (2000), Threshold criterion for debris-flow initiation due to channel bed failure, in *Debris-Flow Hazards Mitigation: Mechanics, Prediction, and Assessment: Proceedings of the 2nd International Conference on Debris Flow Hazards Mitigation, Taipei, Taiwan, 16–18 August 2000*, edited by G. F. Wieczorek and N. D. Naeser, pp. 89–97, A. A. Balkema, Rotterdam, Netherlands.

VanDine, D. F. (1985), Debris flows and debris torrents in the Southern Canadian Cordillera, *Can. Geotech. J.*, *22*, 44–68, doi:10.1139/t85-006.

Wells, W. G. (1985), The influence of fire on erosion rates in California chaparral, in *Proceedings of the Chaparral Ecosystem Conference*, edited by J. J. DeVries, pp. 57–62, Calif. Water Resour. Cent., Santa Barbara.

Wells, W. G. (1987), The effects of fire on the generation of debris flows in southern California, *Rev. Eng. Geol.*, *7*, 105–114.

Wells, W. G., P. M. Wohlgemuth, and A. G. Campbell (1987), Post-fire sediment movement by debris flows in the Santa Ynez Mountains, California, in *Erosion and Sedimentation in the Pacific Rim*, *IAHS Publ.*, *165*, 275–276.

Wondzell, S. M., and J. G. King (2003), Postfire erosional processes in the Pacific Northwest and Rocky Mountain regions, *For. Ecol. Manage.*, *178*, 75–87, doi:10.1016/S0378-1127(03)00054-9.

Yerkes, R. F., and R. H. Campbell (2005), Preliminary geologic map of the Los Angeles 30′ × 60′ quadrangle, southern California, *U.S. Geol. Surv. Open File Rep., 2005-1019*.

Zhang, S. (1993), A comprehensive approach to the observation and prevention of debris flows in China, *Nat. Hazards*, *7*, 1–23, doi:10.1007/BF00595676.

S. H. Cannon, J. W. Kean, and D. M. Staley, U.S. Geological Survey, PO Box 25046, MS 966, Denver, CO 80225, USA. (jwkean@usgs.gov)